

UC San Diego

UC San Diego Electronic Theses and Dissertations

Title

Discovery and Description of New Tyrosinase Inhibitors from Marine Algae and Cyanobacteria

Permalink

<https://escholarship.org/uc/item/9r12z5mc>

Author

He, Yifan

Publication Date

2021

Peer reviewed|Thesis/dissertation

UNIVERSITY OF CALIFORNIA SAN DIEGO

Discovery and Description of New Tyrosinase Inhibitors from Marine Algae and
Cyanobacteria

A thesis submitted for partial satisfaction of the
requirements for the degree Master of Science

in

Marine Biology

by

Yifan He

Committee in charge:

William H. Gerwick, Chair
Pieter Dorrestein
Lena Gerwick

2021

Copyright

Yifan He, 2021
All rights reserved

The thesis of Yifan He is approved, and it is acceptable in quality and form for publication on microfilm and electronically.

University of California San Diego

2021

TABLE OF CONTENTS

THESIS APPROVAL PAGE.....	iii
TABLE OF CONTENTS.....	iv
LIST OF FIGURES.....	v
LIST OF TABLES.....	vii
ACKNOWLEDGEMENTS.....	viii
ABSTRACT OF THE THESIS.....	x
CHAPTER ONE: INTRODUCTION.....	1
CHAPTER TWO: BROAD SCREENING IN SEARCH OF COMPOUNDS WITH SIGNIFICANT TYROSINASE INHIBITORY ACTIVITY.....	17
CHAPTER THREE: SCYTONEMIN MONOMER (ScyM) CASE STUDY: EXAMINING THE INHIBITORY POTENTIAL AND INHIBITION MODE OF SCYTONEMIN MONOMER AGAINST TYROSINASE ENZYME.....	31
CHAPTER FOUR: CONCLUSION.....	74

LIST OF FIGURES

Figure 1.1. Selected marine natural products and/or their clinically useful derivatives.	3
Figure 1.2. A simplified graphic flow chart explaining formation of melanin and freckles in human skin.....	5
Figure 1.3. Involvement of tyrosinase in the melanogenesis pathway (production of eumelanin and pheomelanin).....	6
Figure 1.4. Visualization of Mushroom tyrosinase (<i>Agaricus bisporus</i>) catalytic site, with copper ions coordinated by His61, His85, His94, His259, His263 and His296 amino acid residues	9
Figure 1.5. Selected examples of natural product (NP) tyrosinase inhibitors.	10
Figure 1.6. Structure of potent tyrosinase inhibitor oscillapeptin G isolated from a marine cyanobacterium.....	11
Figure 2.1. Visualization of different extent of tyrosinase inhibition using KA with an increasing concentration gradient.....	19
Figure 2.2. Simplified melanin biosynthesis pathway with tyrosinase catalyzing two of the early steps.	19
Figure 2.3. Layout of the colorimetric assay for screening for tyrosinase inhibition using 96-well microplates.....	21
Figure 2.4. Chemical structure of kojic acid (KA), the positive control used in the tyrosinase inhibitory assay.....	22
Figure 2.5. Tyrosinase inhibitory activity of KA in a dose-dependent manner	25
Figure 2.6. Tyrosinase inhibitory activity of the best candidates from the broad screening at 10 $\mu\text{g/mL}$	25
Figure 2.7. Temporal shift of OD readings for: (A) blank with tyrosinase enzyme, (B) blank without enzyme, (C) KA with enzyme, (D) KA without enzyme, (E) ScyM with enzyme, and (F) ScyM without enzyme.....	27
Figure 3.1. A diagram showing the biosynthesis pathway of scytonemin in <i>Nostoc punctiforme</i> ATCC 29133 and corresponding gene products involved in the biochemical steps.....	35
Figure 3.2. Structure of scytonemin monomer (ScyM) used in this study.....	36
Figure 3.3. Simplified synthetic method to produce ScyM using 3,4-dihydrocyclopenta[b]indol-2(1H)-one and 4-hydroxybenzaldehyde	38
Figure 3.4. Liquid chromatography and mass spectrometry (LCMS) spectra of the crude ScyM product in the positive ionization mode.....	42
Figure 3.5. MS ² spectrum of scytonemin monomer peak in positive mode electrospray ionization (+ESI) with potential fragmentation of [M - 28]	43
Figure 3.6. LCMS spectra of post-HPLC purified ScyM in the positive ionization mode	44
Figure 3.7. Re-check of LCMS analysis of crude ScyM in the positive ionization mode	45
Figure 3.8. HMBC and HSQC correlations for scytonemin monomer in DMF-d ₇	47
Figure 3.9. Dose-dependent percent inhibition against tyrosinase over time for: (A) Scytonemin monomer (ScyM); (B) Kojic acid (KA); (C) ScyM and KA at low concentrations at which ScyM completely dissolves and does not have potential solubility problems.....	48
Figure 3.10. Predicted curves of tyrosinase inhibitory effect versus inhibitor concentration. (A) Scytonemin monomer (ScyM); (B) Kojic acid (KA).....	52
Figure 3.11. Illustration of a typical isobologram-based drug interaction analysis	53
Figure 3.12. Isobologram analysis of interactions of ScyM and KA in tyrosinase inhibition	55
Figure 3.13. Lineweaver-Burk plots for inhibition against Mushroom Tyrosinase of A) KA, and B) ScyM.....	57

Figure 3.14. The binding conformation of L-DOPA (magenta), kojic acid (yellow), ScyM with best binding score (green) and ScyM with second-best binding score (blue)	60
Figure 3.15. The binding conformation of ScyM with best binding score (green), ScyM with second-best binding score (blue) and ScyM-OMe (brown)	62
Figure 3.16. Dose dependent percent inhibition of mushroom tyrosinase by scytonemin and kojic acid over time.	64
Figure 3.17. Predicted ligand interaction of scytonemin and mushroom tyrosinase based on spatial orientation with highest binding score from docking experiment.	66
Figure 3.18. Screening result from DPPH assay showing scytonemin monomer (ScyM) with modest antioxidant activity and the positive control Trolox	67

LIST OF TABLES

Table 2.1. Percent inhibition by kojic acid at various final concentrations.....	24
Table 3.1. ¹ H and ¹³ C NMR Spectroscopic Data of Scytonemin Monomer (ScyM) in DMF-d ₇	46
Table 3.2. Kinetic and inhibition constants of Tyrosinase by KA and ScyM.	50
Table 3.3. Mushroom tyrosinase inhibitory effects of selected compounds from previous publications, in comparison with the positive control KA and the compound of interest ScyM	51
Table 3.4. Results for compounds of interest from docking assays with mushroom tyrosinase enzyme, including binding energies and common ligand interactions with the binding pocket atoms..	59

ACKNOWLEDGEMENTS

This work would not have been possible without the support of many people. I would like to first acknowledge Professor William H. Gerwick for his support as the chair of my committee. From general guidance in experiment design, to detailed suggestions on various specific problems; from patient advice and revision on my writing pieces that were so lack of refinement, to moral support when I was experiencing anxiety due to delayed experiment progress during pandemic, he has proved again and again that he is the greatest mentor of all time. I cannot appreciate more for all the opportunities and help that he has provided in this amazing laboratory.

I would also like to acknowledge Dr. Lena Gerwick for her support as my other mentor in the laboratory, and the entire Gerwick lab for their help and support during my program. Special thanks to Dr. Hyunwoo Kim for always being a valuable resource of information over this one year and a half. And thanks to Dr. Evgenia Glukhov for the tutorial of various instruments in our laboratory and the cytotoxicity assays performed in this study. Thanks to Dr. Mitchell Christy for the initial assistance with MOE program and advice on molecular docking study.

I want to thank our previous visiting scholars, especially Dr. KiYong Lee for the assistance of preliminary ideas on the experimental setup and the assay validation of broad screening in Chapter 2. Also, thank Dr. Yi Zhang for helping me get familiar with screening projects.

I would like to acknowledge Dr. Tak Suyama for re-synthesizing the active compound scytonemin monomer after the depletion of material. My results and analysis would be impossible to report without his generous supply of more of this raw material.

I would also like to acknowledge Dr. Brendan M. Duggan for the assistance in running the 600MHZ NMR instrument at Skaggs School of Pharmacy and Pharmaceutical Sciences.

Chapter 2 and Chapter 3, in part, are currently being prepared for submission for publication of the material. Yifan He, Tak Suyama, Hyunwoo Kim, Evgenia Glukhov and William H. Gerwick. The dissertation author was the primary investigator and author of this material.

Last but not the least, I am deeply thankful for all my family members and my girlfriend Jolene who served as my emotional support during the program and the pandemic.

ABSTRACT OF THE THESIS

Discovery and Description of New Tyrosinase Inhibitors from Marine Algae and Cyanobacteria

by

Yifan He

Master of Science in Marine Biology

University of California San Diego, 2021

Professor William H. Gerwick, Chair

Tyrosinase, an important oxidase involved in the primary immune response in humans, can sometimes become problematic as it can catalyze undesirable oxidation reactions. Therefore, for decades there has been a strong pharmaceutical interest in the discovery of novel inhibitors of this enzyme. Recent studies have also indicated that tyrosinase inhibitors can potentially be used in the treatment of melanoma cancer. Over the years, a number of new tyrosinase inhibitors have been isolated from various natural sources, although marine natural products (MNPs) have contributed only a small number of promising candidates. In this regard, the exploration of tyrosinase inhibitors from marine cyanobacteria

has been especially understudied. This research therefore mainly focused on the discovery of new tyrosinase inhibitors of marine cyanobacterial and algal origins. A colorimetric fungal tyrosinase inhibitory assay was used to screen extracts, fractions, and pure compounds for anti-tyrosinase activity. Scytonemin monomer (ScyM), the monomeric structure of the well-known cyanobacterial sunscreen pigment scytonemin (Scy), was found to have the highest tyrosinase inhibitory score and was more potent than the commercial standard inhibitor kojic acid (KA). Consequently, ScyM has become our top compound and we explored a series of follow-up studies on its structure, inhibitory power, and mode of inhibition.

CHAPTER ONE

INTRODUCTION

I. Short story of natural product and marine natural product in drug discovery

The use of natural substances for medicinal purposes started as early as 2600 B.C., long before humans understood the concept of pharmacology (Cragg and Newman, 2005). Many of the highly specialized secondary metabolites of plants, which are often evolutionarily selected molecules that benefit the organism's well-being or fecundity, were already being used for curing illness in ancient times. And some specific ones, such as the oils of *Glycyrrhiza glabra* (licorice) and *Papaver somniferum* (poppy juice), are still being used today to treat health conditions including cough, infection, etc. (Cragg and Newman, 2005). Now, thousands of years later, we are still exploring plants, animals, and microbial life for novel medicines from natural sources. This field of investigation is known as “natural products research” or “pharmacognosy”.

By late 2019, about two thirds of all approved drugs were somehow related to NPs: either NPs themselves, NP derivatives, or synthetic drugs inspired by NP pharmacophores (Newman and Cragg, 2020). This again illustrates the long-lived importance of NPs in human health. For example, well known natural medicines include aspirin (derived from salicin, of the willow tree bark), morphine (isolated from the opium poppy), quinine (isolated from the bark of *Cinchona* trees), and penicillin (isolated from *Penicillium fungi*). It is widely accepted that the discovery of penicillin changed the face of modern medicine, and initiated a golden era of antibiotics in medicine. This brought greater attention and importance for NP research throughout the entire scientific community (Fleming, 1944; Clark, 1996).

Nevertheless, while the NP field has been in existence for a considerable time, the field of marine natural product (MNP) research is relatively young. One of the first reports of a MNP possessing significance to human health was the isolation of prostaglandins from the gorgonian coral *Plexaura homomalla*; however, this discovery dates back only to the 1960s (Weinheimer and Spraggins, 1969). A critical reason for this delayed development of MNP study was the restricted accessibility to oceans compared to terrestrial sources. Consequently, early MNP discovery focused on the most noticeable and easily collectable organisms near the intertidal and coastal regions, like red algae, sponges, and soft corals (Gerwick and Moore, 2012). It was not until the invention of SCUBA and subsequent deep-sea diving vessels that MNP studies were expanded to a larger scope and started to cover deeper water creatures. (Gerwick and Fenner, 2013). Accordingly, marine natural products became a much more well-established subdiscipline of natural products research by the end of 20th century, with thousands of compounds identified and three specialized tracks developed: marine biomedicines, marine toxins, and marine chemical ecology (Faulkner, 2000). For example, trabectedin (also known as ecteinascidin 743 or ET-743, Figure 1.1) is one of the most famous compounds of a marine origin, which is approved for use as an anti-tumor drug. The history of this compound is legendary as it took many years between its isolation from the tunicate *Ecteinascidia turbinata*, the structural elucidation thereafter, until its final approval as a drug by the FDA in 2015 (Barone *et al.*, 2017).

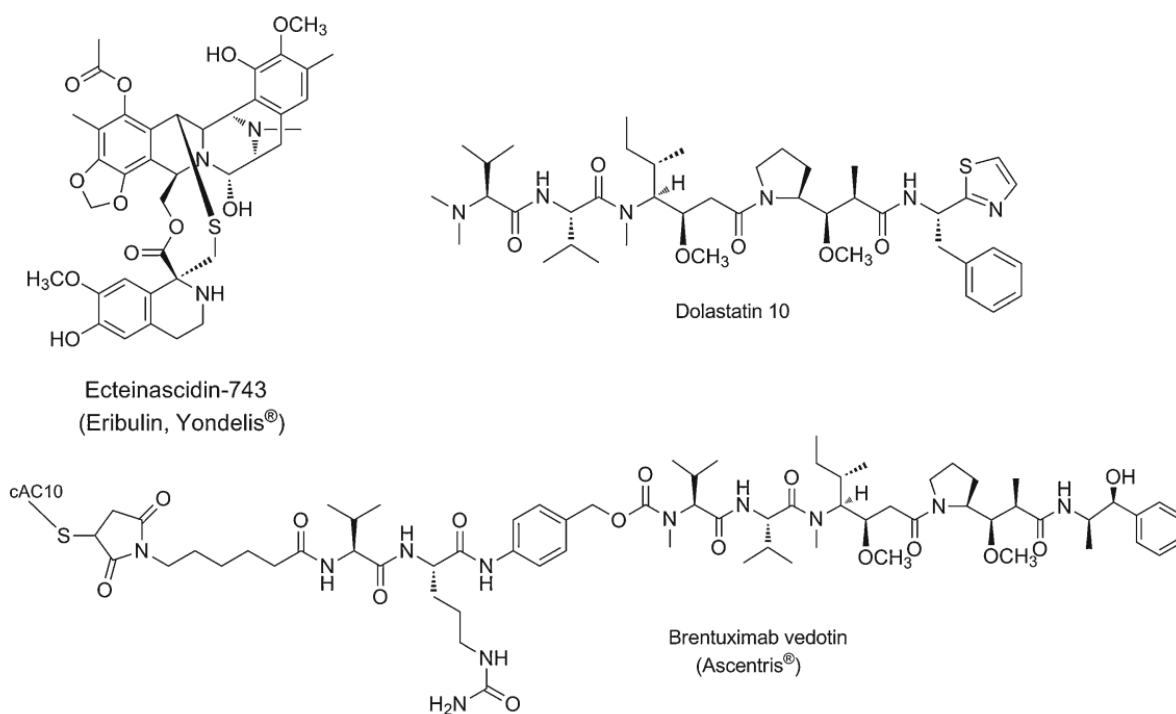


Figure 1.1. Selected marine natural products and/or their clinically useful derivatives.

Besides the progress that was made on marine organisms from a broader diversity of habitats, with developing technologies there was another important trend. MNP researchers started to pay attention to smaller and smaller organisms that had formerly escaped collection and investigation (Gerwick and Moore, 2012). Microorganisms, such as marine fungi, marine cyanobacteria, and diverse other groups of marine eubacteria, were also examined for metabolites with medically relevant bioactivities. One story of MNP success in drug discovery from bacteria involves the identification of dolastatin 10 (Figure 1.1), a highly cytotoxic product that was originally isolated from the sea hare *Dolabella auricularia* but later found to be actually produced by the cyanobacterium *Symploca* sp. (Pettit *et al.*, 1987; Luesch *et al.*, 2001). With considerable antiproliferative properties, dolastatin 10 and its analogs were assessed in a number of clinical trials but found in all cases too toxic to be directly used in the treatment of cancer, primarily as a result of causing peripheral neuropathy (Pitot *et al.*, 1999). As another approach, in 2010 a dolastatin 10 analog was conjugated to an antibody, which would help target the delivery of this active molecule directly to tumor cells

with the appropriate cancer cell epitope. This mechanism was proven to be successful and resulted in a powerful and accurate cytotoxic effect without interference of non-tumor cells. The conjugated drug, given the name brentuximab vendotin (Figure 1.1), was approved for treating systemic anaplastic large cell lymphoma and relapsed Hodgkin's lymphoma (Senter and Sievers, 2012).

Overall, despite the promising potency observed in many preliminary studies, there are certainly obstacles and challenges remaining in the field, such as the frequently-met practical problem of limited natural yields of the materials of interest. This issue of limited supply has created many difficulties for MNPs to be fully revealed for their potential in actual clinical evaluations and development (Gerwick and Moore, 2012). However, the future is bright and full of possibilities. Finer and finer omics studies have been developed during the last 20 years, and great advances have been made in analytical techniques involving metabolomics, genomics, and proteomics, such as molecular networking and genome mining (Chu *et al.*, 2020; Stuart *et al.*, 2020). These biotechnological tools, complementary to other traditional metabolomics approach in MNP study, have all been promoting a better understanding of the biosynthetic pathways that code for secondary metabolites in marine microbes. As a result, marine microorganisms have been increasingly recognized as a particularly productive source of unique secondary metabolites (Gerwick and Moore, 2012). The elucidation of the biosynthesis of microbial MNPs, as well as many other important achievements currently happening in the MNP research field, altogether contribute to the concept of natural products and drug discovery in the “genomic era” (Shen *et al.*, 2021). The “next golden age” might be awaiting!

II. Melanin biosynthesis, tyrosinase, and the linkage with natural product research

The market for skin-whitening products, especially in Asian countries, such as China, India, and Japan, is experiencing unprecedented growth (Grand View Research, 2019). The fundamental mechanism of skin-whitening or dark-spot treatment products, is to reduce the amount of melanin in the outer layer of skin called the epidermis. Produced in specialized cells known as melanocytes through the process of melanogenesis, melanin is a group of natural pigments that determines our skin, eye, and hair colors by the quantity and distribution of its container organelle, the “melanosomes” (Pillaiyar *et al.*, 2017; Qian *et al.*, 2020). Under normal physiological conditions, melanin production or melanogenesis, plays a crucial role in protecting us from UV-induced skin damage caused by harmful amounts of UV light exposure (Brenner, 2008). However, it can become problematic when melanin is over-produced or is unevenly distributed, leading to undesirable skin problems include freckles, age spots (Pillaiyar *et al.*, 2017), and melanoma (Brenner, 2008). Therefore, there is a desire to regulate the melanogenesis pathway to avoid deleterious effects while maintaining normal function.

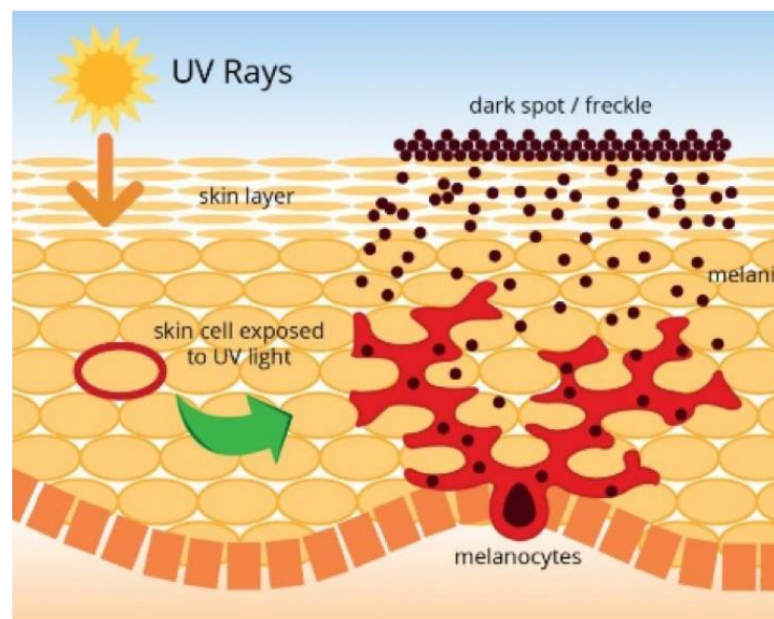


Figure 1.2. A simplified graphic flow chart explaining formation of melanin and freckles in human skin. Figure derived from Maxwhite.com, 2016.

In vertebrates, melanogenesis involves a series of reactions that are catalyzed by multiple enzymes. As shown in Figure 1.3, the pathway is initiated by the oxidation of the starting material L-tyrosine (or L-DOPA) to dopaquinone by the enzyme tyrosinase (D’Mello *et al.*, 2016). The resulting quinone then serves as the substrate for subsequent steps in the pathway that eventually leads to the production of melanin(s). In this regard, the formation of dopaquinone catalyzed by tyrosinase has been considered to be the rate-limiting step in the melanogenesis pathway. This is because the remaining steps can proceed spontaneously at a physiological pH as long as dopaquinone is present (Pillaiyar *et al.*, 2017).

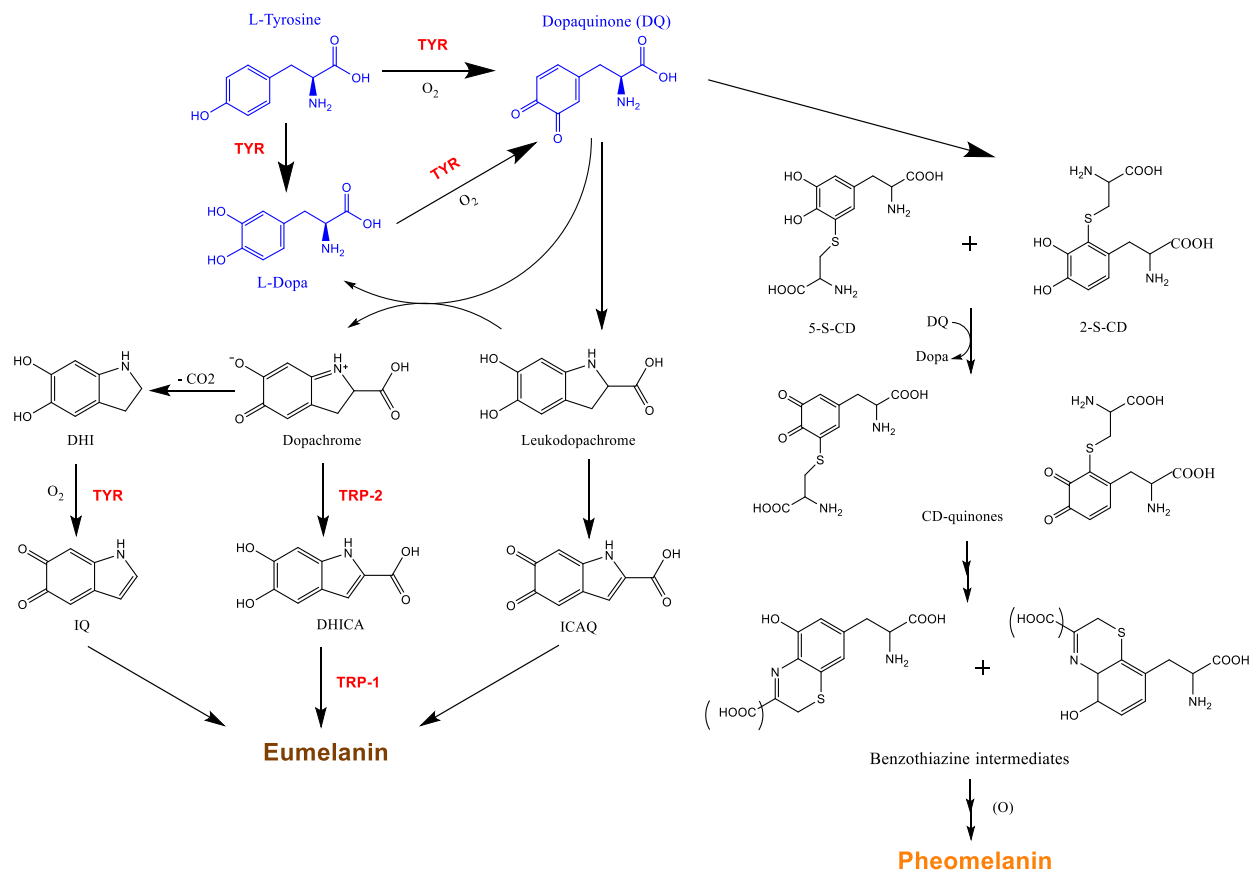


Figure 1.3. Involvement of tyrosinase in the melanogenesis pathway (production of eumelanin and pheomelanin). TYR stands for Tyrosinase, TYP-1 and TYP-2 refers to two tyrosinase-related proteins. Figure recreated from Pillaiyar *et al.*, 2017.

Due to the important role tyrosinase plays in the biosynthesis of melanin, it has become a potential target to treat melanin overproduction in humans. The search for

tyrosinase inhibitors to restrain the activity of this enzyme, so as to restrict the production of melanin, has been long considered a good approach to treat hyperpigmentation. However, even after being studied for a considerable time, tyrosinase inhibitors that are currently used in skin care products still have drawbacks: patients with sensitive skin may develop dermatitis, allergy, and even more severe symptoms, such as carcinogenesis (Cho *et al.*, 2020). Therefore, it remains a hot topic in the pharmaceutical field to find more and better tyrosinase inhibitors.

Besides being added to cosmetic products for skin whitening, tyrosinase inhibitors also have great biomedical value as a potential cure for a specific skin cancer known as melanoma. Melanoma is a type of skin cancer originating from abnormally functioning melanocytes due to genetic defects or UV-induced damage. This uncontrolled melanoma cell replication causes a failure in regulation of melanin synthesis and proper transportation to keratinocytes in the epidermis, which in turn leads to melanin accumulation (Eddy *et al.*, 2020). Furthermore, the buildup of melanin inside melanoma cells can hinder the most common therapies used to treat cancer (i.e. radiotherapy, chemotherapy, photodynamic therapy etc.) (Buitrago *et al.*, 2016). This may partially explain why melanoma accounts for the lowest number of cases but the highest mortality among all three main types of skin cancer (Liu *et al.*, 2014). Fortunately, recent studies have shown that by targeting tyrosinase for inhibition and thereby stopping or decreasing melanin production, the sensitivity of melanoma cells to radiation and other therapies can be restored. This discovery therefore constitutes a promising adjuvant approach to treat melanoma (Buitrago *et al.*, 2016), broadens the application for tyrosinase inhibitors in human health, and further increases the demand for more novel candidates.

Tyrosinase (TYR), the rate-limiting enzyme in melanogenesis that affects the quantity of melanin synthesized in various organisms (D'Mello *et al.*, 2016), has been isolated and

purified from different sources such as plants, animals, and microorganisms. It has been reported that some compounds have distinct activities to different tyrosinases, depending on the source of this enzyme (Zolghadri *et al.*, 2019). For instance, a recent study showed that thiamidol inhibited mushroom tyrosinase weakly, but was a potent inhibitor of human tyrosinase with an excellent IC_{50} value of 1.1 μ M (Mann *et al.*, 2018). However, because of the high similarity and homology of the tyrosinase from the edible mushroom *Agaricus bisporus* compared to human tyrosinase, it has become a major and economical substitute that is commonly used in the initial screening stage for new tyrosinase inhibitors (Ismaya *et al.*, 2011). For these reasons, it was also the tyrosinase used in the study reported in this thesis.

First isolated in 1895 (Bourquelot and Bertrand, 1895), mushroom tyrosinase has an H_2L_2 tetramer structure, where the H subunit contains a binuclear copper site (Figure 1.4), with each copper ion coordinated by three His residues through similar distance (Ismaya *et al.*, 2011; Lima *et al.*, 2014). It was claimed that these interactions with Cu^{2+} restrict the rotation of the histidine residues and reduce flexibility (Karakaya *et al.*, 2019). This stabilized copper site meanwhile serves as the typical catalytic site of tyrosinase and is spatially adjacent to the substrate binding pocket (Ismaya *et al.*, 2011). With its crucial catalytic property and proximity to the substrate binding pocket, the copper-binding site of tyrosinase has provided great insights into the potential inhibitory mechanism of various tyrosinase inhibitors. More specifically, several inhibitors function as copper chelators (Chang, 2009), a concept that has been investigated intensively over the past few decades.

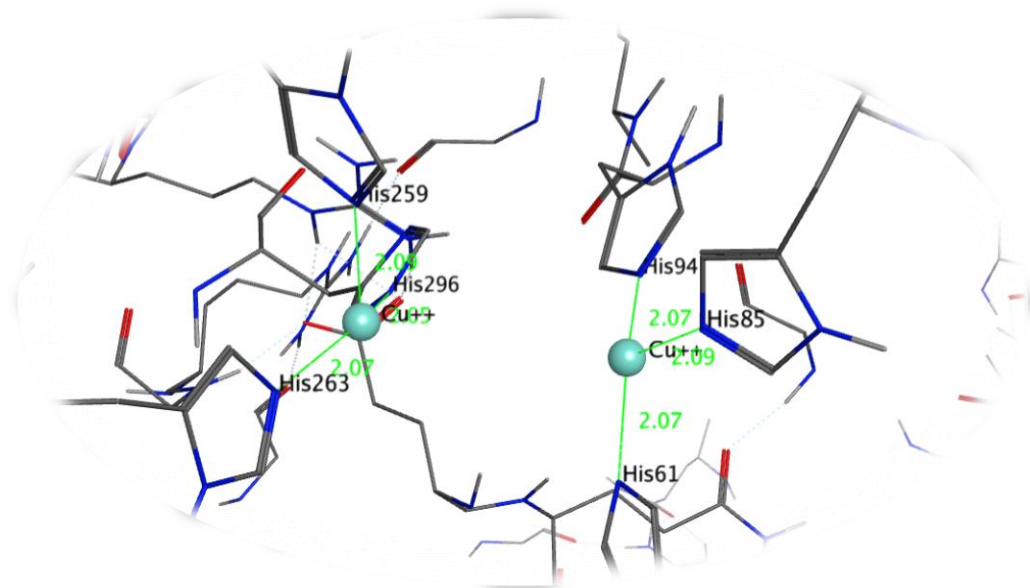


Figure 1.4. Visualization of Mushroom tyrosinase (*Agaricus bisporus*) catalytic site, with copper ions coordinated by His61, His85, His94, His259, His263 and His296 amino acid residues. All distances shown in green are in Å.

Mechanistically, there are four types of tyrosinase inhibitors. Competitive inhibitors bind to a free enzyme and prevent substrate binding to the enzyme active site. Uncompetitive inhibitors can only bind to the enzyme-substrate complex. Mixed inhibitors can bind to both a free enzyme and the enzyme-substrate complex as a combination of previous two types. Finally, non-competitive inhibitors bind to a free enzyme and an enzyme-substrate complex with the same equilibrium constant as a special case of mixed-type inhibition (Zolghadri *et al.*, 2019). A competitive inhibitor could be a copper chelator, non-metabolizable analog, or derivatives of the true substrate (Chang, 2009). Many aromatic acids, phenolic and poly-phenolic compounds, as well as a few non-aromatic compounds, are classified as copper chelators that bind to tyrosinase competitively (see Figure. 1.5) (Zolghadri *et al.*, 2019). Non-competitive and mixed inhibition are frequent modes observed in kinetic studies of mushroom tyrosinase activities. Examples of mixed inhibitors include phthalic acid and kojic acid, while propanoic acid and thiazole derivatives are instances of uncompetitive and non-competitive inhibitors, respectively (Gheibi *et al.*, 2009; Deri *et al.*, 2016; Hassani *et al.*, 2016; Saeed *et al.*, 2017).

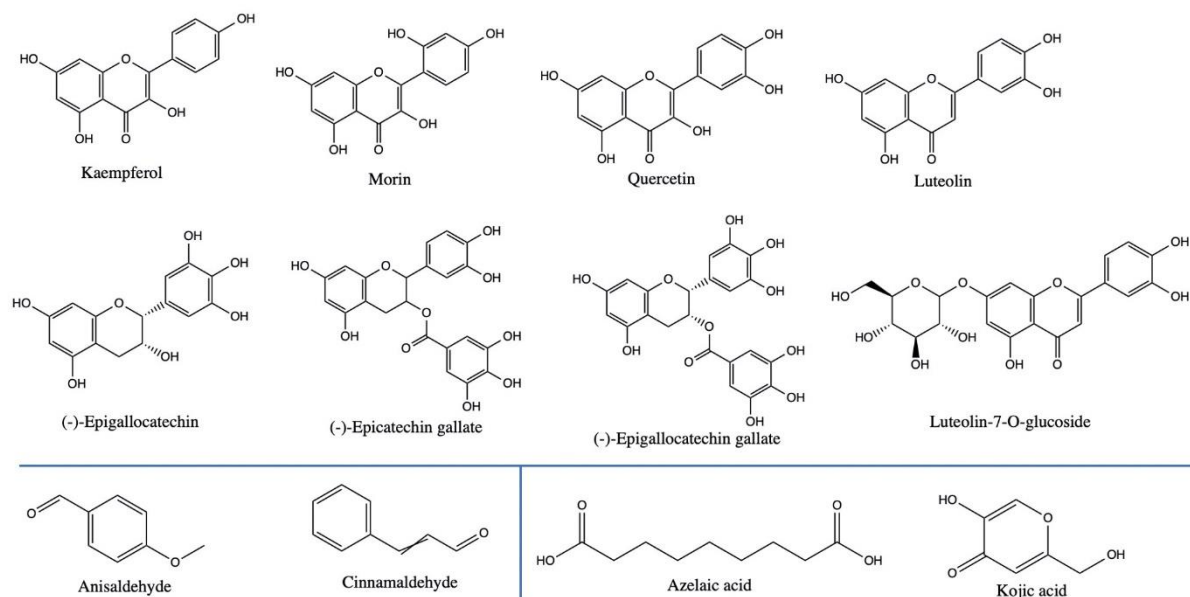


Figure 1.5. Selected examples of natural product (NP) tyrosinase inhibitors.

Natural products have been significant sources of tyrosinase inhibitors. This is partially because flavonoids and flavonoids derivatives, which belong to the diverse group of polyphenols from various higher plant sources, accounts for a considerable proportion of tyrosinase inhibitors discovered so far (Zolghadri *et al.*, 2019). For instance, kaempferol, morin and quercetin, as well as gallates, gallic acid and its esters (Figure 1.5), all are considered to fall in the category of flavonoids and flavonoids derivatives isolated from plants (Kim and Uyama, 2005). Additionally, some aldehydes, such as anisaldehyde and cinnamaldehyde, were also isolated from plants and characterized as tyrosinase inhibitors (Kubo and Kinst-Hori, 1998; Lee *et al.*, 2000). Besides higher plants, several compounds from fungal sources have also been discovered and reported for their tyrosinase inhibitory activity (Nazzaro-Porro and Passi, 1978; Sharma *et al.*, 2004; Morimura *et al.*, 2007). The most prominent fungal-derived inhibitor is kojic acid (KA), which is a metabolite produced mainly by fungi belonging to the genus *Aspergillus* (Lima *et al.*, 2014). It is also the most widely used skin-whitening agent in various cosmetic products (Gillbro and Olsson, 2011). For this reason, KA has been chosen as the positive control in many tyrosinase inhibition

studies, including the present one that will be introduced in detail in Chapter 2. Regarding its inhibitory mechanism, there are contradictory theories described in scientific publications for KA where it is described as either a competitive or mixed inhibitor of mushroom tyrosinase (Noh *et al.*, 2009; Bochot *et al.*, 2014; Lima *et al.*, 2014). A relatively recent study clarified this issue through techniques including ligand co-crystallization, molecular modeling, binding constant analysis and kinetic experiments, and confirmed that KA acts as a mixed inhibitor (Deri *et al.*, 2016).

Nevertheless, despite the fact that a number of new tyrosinase inhibitors have been isolated from various natural sources over the years, there were only a few promising candidates that come from marine natural products (MNPs). Fucoxanthin, isolated from the marine alga *Laminaria japonica*, was found to suppress tyrosinase activity in UVB-irradiated guinea pig skin and melanogenesis in UVB-irradiated mice (Shimoda *et al.*, 2010). N-Acyl dehydrotyrosine derivatives, produced by marine Gram-negative bacterium, were also reported to inhibit tyrosinase *in vitro* (Deering *et al.*, 2016). So far, only one compound was discovered from a marine cyanobacterium to inhibit tyrosinase, namely the cyclic peptide oscillapeptin G (Sano *et al.*, 1996, see Figure 1.6 for structure). This clearly reveals a lack of investigation of marine cyanobacteria for new tyrosinase inhibitors, and this fact was partly the inspiration for the current study.

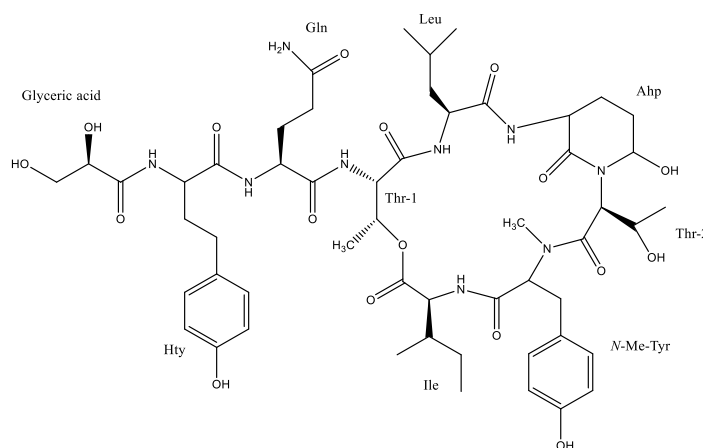


Figure 1.6. Structure of potent tyrosinase inhibitor oscillapeptin G isolated from a marine cyanobacterium. Figure redrawn from Sano *et al.*, 1996.

III. General thesis contents

With the demand for more effective tyrosinase inhibitors and the under-explored nature of marine algae and cyanobacteria for compounds with this activity, I initiated a screening program for novel tyrosinase inhibitors of marine cyanobacterial and algal origin. These could potentially be used as skin whitening agents or treatment of melanoma in the future.

Chapter 2 describes my efforts to screen the Gerwick extract library and pure compound library against mushroom tyrosinase (*A. bisporus*). Summarized in this chapter are explanation of the methods and concepts behind this screening effort, the validation of the colorimetric assay used for the screening, and the screening results.

The top hit identified from this screen, scytonemin monomer (ScyM), is a pure compound in our library. Furthermore, it is proposed as the last-step precursor in the biosynthesis of the cyanobacterial sunscreen pigment ‘scytonemin’. As a result, it was selected for more extensive analysis and resulted in the work detailed in Chapter 3. Further biochemical assay work, in conjunction with in-silico docking and enzyme kinetics study, suggests that ScyM shows a slowly reversible mixed-type inhibition against mushroom tyrosinase, with better inhibitory potency than the commercially available standard tyrosinase inhibitor Kojic Acid (KA). This excellent *in vitro* performance of ScyM makes it a novel candidate for applications such as a skin whitening agent or an adjuvant therapy for melanoma. Thus, it would be interesting to test for its tyrosinase inhibitory activity in *in-vivo* models in the future.

References:

- Barone A, Chi D-C, Theoret MR, Chen H, He K, Kufrin D, Helms WS, Subramaniam S, Zhao H, Patel A, Goldberg KB, Keegan P, Pazdur R. (2017) FDA approval summary: Trabectedin for unresectable or metastatic liposarcoma or leiomyosarcoma following an anthracycline-containing regimen. *Clin Cancer Res.* 23(24):7448–7453.
- Bochot C, Gouron A, Bubacco L, Milet A, Philouze C, Réglie M, Serratrice G, Jamet H, Belle C. (2014) Probing kojic acid binding to tyrosinase enzyme: insights from a model complex and QM/MM calculations. *Chem Commun (Camb).* 50(3):308–310.
- Bourquelot E, Bertrand A (1895) Le bluissement et le noircissement des champignons. *Comp Rend Soc Biol.* 2:582–4.
- Brenner M, Hearing VJ. (2008) The protective role of melanin against UV damage in human skin. *Photochem Photobiol.* 84:539–49.
- Buitrago E, Hardré R, Haudecoeur R, Jamet H, Belle C, Boumendjel A, Bubacco L, Réglie M. (2016) Are human tyrosinase and related proteins suitable targets for melanoma therapy? *Curr Top Med Chem.* 16(27):3033–3047.
- Chang T-S. (2009) An updated review of tyrosinase inhibitors. *Int J Mol Sci.* 10(6):2440–2475.
- Cho K, Ryu CS, Jeong S, Kim Y. (2020) Potential adverse effect of tyrosinase inhibitors on teleosts: A review. *Comp Biochem Physiol C Toxicol Pharmacol.* 228(108655):108655.
- Chu L, Huang J, Muhammad M, Deng Z, Gao J. (2020) Genome mining as a biotechnological tool for the discovery of novel marine natural products. *Crit Rev Biotechnol.* 40(5):571–589.
- Clark, A.M. (1996) Natural products as a resource for new drugs. *Pharm. Res.* 13(8): 1133-1141.
- Cragg GM, Newman DJ. (2005) Biodiversity: A continuing source of novel drug leads. *Pure Appl Chem.* 77(1):7–24.
- Deering RW, Chen J, Sun J, Ma H, Dubert J, Barja JL, Seeram NP, Wang H, Rowley DC. (2016) N-acyl dehydrotyrosines, tyrosinase inhibitors from the marine bacterium *Thalassotalea* sp. PP2-459. *J Nat Prod.* 79(2):447–450.
- Deri B, Kanteev M, Goldfeder M, Lecina D, Guallar V, Adir N, Fishman A. (2016) The unravelling of the complex pattern of tyrosinase inhibition. *Sci Rep.* 6:34993.
- D'Mello SA, Finlay GJ, Baguley BC, Askarian-Amiri ME. (2016) Signaling Pathways in Melanogenesis. *Int J Mol Sci.* 17(7):1144.
- Eddy K, Shah R, Chen S. (2020) Decoding melanoma development and progression: Identification of therapeutic vulnerabilities. *Front Oncol.* 10:626129.

- Faulkner, D.J. (2000) Highlights of marine natural products chemistry (1972-1999). *Nat. Prod. Rep.* 17(1): 1-6.
- Fleming, A. (1944) The discovery of penicillin. *Br. Med. Bull.* 2(1): 4-5.
- Gerwick WH, Fenner AM. (2013) Drug discovery from marine microbes. *Microb Ecol.* 65(4):800–806.
- Gerwick WH, Moore BS. (2012) Lessons from the past and charting the future of marine natural products drug discovery and chemical biology. *Chem Biol.* 19(12):1631.
- Gheibi N, Saboury AA, Haghbeen K, Rajaei F, Pahlevan AA. (2009) Dual effects of aliphatic carboxylic acids on cresolase and catecholase reactions of mushroom tyrosinase. *J Enzyme Inhib Med Chem.* 24(5):1076–1081.
- Gillbro JM, Olsson MJ. (2011) The melanogenesis and mechanisms of skin-lightening agents--existing and new approaches: Melanogenesis and skin-lightening agents. *Int J Cosmet Sci.* 33(3):210–221.
- Grand View Research. (2019) Skin Lightening Products Market Size, Share & Trends Analysis Report By Product (Cream, Cleanser, Mask), By Nature (Synthetic, Natural, Organic), By Region, And Segment Forecasts, 2019 - 2025.
- Hassani S, Haghbeen K, Fazli M. (2016) Non-specific binding sites help to explain mixed inhibition in mushroom tyrosinase activities. *Eur J Med Chem.* 122:138–148.
- Ismaya WT, Rozeboom HJ, Weijn A, Mes JJ, Fusetti F, Wichers HJ, Dijkstra BW. (2011) Crystal structure of *Agaricus bisporus* mushroom tyrosinase: identity of the tetramer subunits and interaction with tropolone. *Biochemistry.* 50(24):5477–5486.
- Karakaya G, Türe A, Ercan A, Öncül S, Aytemir MD. (2019) Synthesis, computational molecular docking analysis and effectiveness on tyrosinase inhibition of kojic acid derivatives. *Bioorg Chem.* 88(102950):102950.
- Kim Y-J, Uyama H. (2005) Tyrosinase inhibitors from natural and synthetic sources: structure, inhibition mechanism and perspective for the future. *Cell Mol Life Sci.* 62(15):1707–1723.
- Kubo I, Kinst-Hori I. (1998) Tyrosinase inhibitors from anise oil. *J Agric Food Chem.* 46(4):1268–1271.
- Lee S-E, Kim M-K, Lee S-G, Ahn Y-J, Lee H-S. (2000) Inhibitory effects of *Cinnamomum cassia* bark-derived mateCMLS, Cell. Mol. Life Sci. Vol. 62, 2005 Research Article 1721 rials on mushroom tyrosinase. *Food Sci. Biotechnol.* 9: 330– 333
- Lima CR, Silva JRA, de Tássia Carvalho Cardoso E, Silva EO, Lameira J, do Nascimento JLM, do Socorro Barros Brasil D, Alves CN. (2014) Combined kinetic studies and computational analysis on kojic acid analogous as tyrosinase inhibitors. *Molecules.* 19(7):9591–9605.

- Liu Y, Sheikh MS. (2014) Melanoma: Molecular pathogenesis and therapeutic management. *Mol Cell Pharmacol.* 6(3):228.
- Luesch H, Moore RE, Paul VJ, Mooberry SL, Corbett TH (2001) Isolation of dolastatin 10 from the marine cyanobacterium *Symploca* species VP642 and total stereochemistry and biological evaluation of its analogue symplostatin 1. *J Nat Prod* 64:907–910
- Mann T, Gerwat W, Batzer J, Eggers K, Scherner C, Wenck H, Stäb F, Hearing VJ, Röhm K-H, Kolbe L. (2018) Inhibition of human tyrosinase requires molecular motifs distinctively different from mushroom tyrosinase. *J Invest Dermatol.* 138(7):1601–1608.
- Maxwite: Ingredients & Mechanism of Action. 2016. Maxwite.com. [accessed 2021 Aug 25]. <http://www.maxwite.com/mechanism-of-action.php>.
- Morimura K, Yamazaki C, Hattori Y, Makabe H, Kamo T, Hirota M. (2007) A tyrosinase inhibitor, Daedalin A, from mycelial culture of *Daedalea dickinsii*. *Biosci Biotechnol Biochem.* 71(11):2837–2840.
- Nazzaro-Porro M, Passi S. (1978) Identification of tyrosinase inhibitors in cultures of *Pityrosporum*. *J Invest Dermatol.* 71(3):205–208.
- Newman DJ, Cragg GM. (2020) Natural products as sources of new drugs over the nearly four decades from 01/1981 to 09/2019. *J Nat Prod.* 83(3):770–803.
- Noh J-M, Kwak S-Y, Seo H-S, Seo J-H, Kim B-G, Lee Y-S. (2009) Kojic acid-amino acid conjugates as tyrosinase inhibitors. *Bioorg Med Chem Lett.* 19(19):5586–5589.
- Pettit GR, Kamano Y, Herald CL, Tuinman AA, Boettner FE, Kizu H, Schmidt JM, Baczynskyj L, Tomer KB, Bontems RJ (1987) The isolation and structure of a remarkable marine animal antineoplastic constituent: dolastatin 10. *J Am Chem Soc* 109:6883–6885
- Pillaiyar T, Manickam M, Namasivayam V. (2017) Skin whitening agents: medicinal chemistry perspective of tyrosinase inhibitors. *J Enzyme Inhib Med Chem.* 32(1):403–425.
- Pitot HC, McElroy EA Jr, Reid JM, Windebank AJ, Sloan JA, Erlichman C, Bagniewski PG, Walker DL, Rubin J, Goldberg RM, Adjei AA, Ames MM (1999) Phase I trial of dolastatin-10 (NSC 376128) in patients with advanced solid tumors. *Clin Cancer Res* 5:525–531
- Qian W, Liu W, Zhu D, Cao Y, Tang A, Gong G, Su H. (2020) Natural skin-whitening compounds for the treatment of melanogenesis (Review). *Exp Ther Med.* 20(1):173–185.
- Saeed A, Mahesar PA, Channar PA, Abbas Q, Larik FA, Hassan M, Raza H, Seo S-Y. (2017) Synthesis, molecular docking studies of coumarinyl-pyrazolinyl substituted thiazoles as non-competitive inhibitors of mushroom tyrosinase. *Bioorg Chem.* 74:187–196.

- Sano T, Kaya K. (1996) Oscillapeptin G, a tyrosinase inhibitor from toxic *Oscillatoria agardhii*. *J Nat Prod.* 59(1):90–92.
- Senter PD, Sievers EL (2012) The discovery and development of brentuximab vedotin for use in relapsed Hodgkin lymphoma and systemic anaplastic large cell lymphoma. *Nat Biotech.* 30:631–637
- Sharma VK, Choi J, Sharma N, Choi M, Seo S-Y. (2004) In vitro anti-tyrosinase activity of 5-(hydroxymethyl)-2-furfural isolated from *Dictyophora indusiata*. *Phytother Res.* 18(10):841–844.
- Shen B, Tang Y, Baltz RH, Gonzalez R. (2021) Introduction to the special issue: “Natural Product Discovery and Development in the Genomic Era: 2021.” *J Ind Microbiol Biotechnol.* 48(3–4). doi:10.1093/jimb/kuab030
- Shimoda H, Tanaka J, Shan S-J, Maoka T. (2010) Anti-pigmentary activity of fucoxanthin and its influence on skin mRNA expression of melanogenic molecules: Suppressive effect of fucoxanthin on melanin synthesis. *J Pharm Pharmacol.* 62(9):1137–1145.
- Stuart KA, Welsh K, Walker MC, Edrada-Ebel R. (2020) Metabolomic tools used in marine natural product drug discovery. *Expert Opin Drug Discov.* 15(4):499–522.
- Weinheimer AJ, Spraggins RL. (1969) The occurrence of two new prostaglandin derivatives (15-epi-PGA₂ and its acetate, methyl ester) in the Gorgonian Chemistry of Coelenterates. XV. *Tetrahedron Lett.* 10(59):5185–5188.
- Zolghadri S, Bahrami A, Hassan Khan MT, Munoz-Munoz J, Garcia-Molina F, Garcia-Canovas F, Saboury AA. (2019) A comprehensive review on tyrosinase inhibitors. *J Enzyme Inhib Med Chem.* 34(1):279–309.

CHAPTER TWO

BROAD SCREENING IN SEARCH OF COMPOUNDS WITH SIGNIFICANT TYROSINASE INHIBITORY ACTIVITY

Abstract

Due to the widespread applications of tyrosinase inhibitors, an appropriate screening method for new tyrosinase inhibitors becomes particularly important. Here, using a validated colorimetric assay, a broad screening of a total of 2619 samples in the Gerwick Laboratory compound library was performed to select materials with the potential for tyrosinase inhibition. The resulting six positive candidates were then further analyzed in a dose-dependent assay to re-confirm their activity and filter out any false-positives. With the combination of these two approaches, the pure compound scytonemin monomer was identified to consistently show significant tyrosinase inhibitory activity, and hence became our compound of interest for further in-depth investigations.

I. Introduction

Tyrosinase inhibitors, by hindering the proper functioning of tyrosinase in various cases, have diverse applications, including cosmetics, medicines and even food technology. With the demand for more tyrosinase inhibitors, *in vitro* assays and screening techniques have been consistently enhanced to provide better sensitivity and accuracy. According to a recent review by Zolghadri (2019), a large variety of methods have been developed and applied by researchers over the years: from the earlier radiometric, spectrophotometric and chromatographic assays, to the relatively more recent electrophoretic and electrochemical

ones. At the same time, it is also important to notice how virtual screening together with computational modeling tools are starting to reveal their unique advantages over traditional *in vitro* assays (Zolghadri *et al.*, 2019). Virtual screening can help reduce the number of compounds of potential interest, and hence, shorten the time required for screening in a large project (Ai *et al.*, 2014). Despite these advances, there is still room for improvement in the precision of putative hits as well as in the breadth of virtual screening due to the limited size of available databases.

To date, the most common method used in the initial screenings of tyrosinase inhibitors is still the classic Spectrophotometric Enzyme Assay. But to save time and material in predicting active compounds from crude extracts in natural product research, such strategy was also developed to be coupled with LC-MS/MS to function as advanced online assay in recent studies (Yang *et al.*, 2018). The spectrophotometric assay generally measures alterations in the intensity of light (UV-vis spectroscopy) absorbed by the reaction solution, and consequently tracks the enzyme reaction of interest. For tyrosinase inhibitory assays, this assay utilizes the concept that tyrosinase catalyzes the oxidation of a substrate, commonly tyrosine/L-Dopa (see Figure 2.2), producing a chromophore that is best detected at 475-510nm (Ha *et al.*, 2007; Lima *et al.*, 2013; Mutschlechner *et al.*, 2018). Therefore, the activity of tyrosinase can be reflected by the change of Optical Density (OD) at a chosen wavelength. And because the wavelengths used for detection falls beneath the visible spectrum for humans, this type of tyrosinase-inhibitor screening method is also known as a colorimetric assay (See Figure 2.1).

Low Tyrosinase activity
/High Inhibition

High Tyrosinase
activity

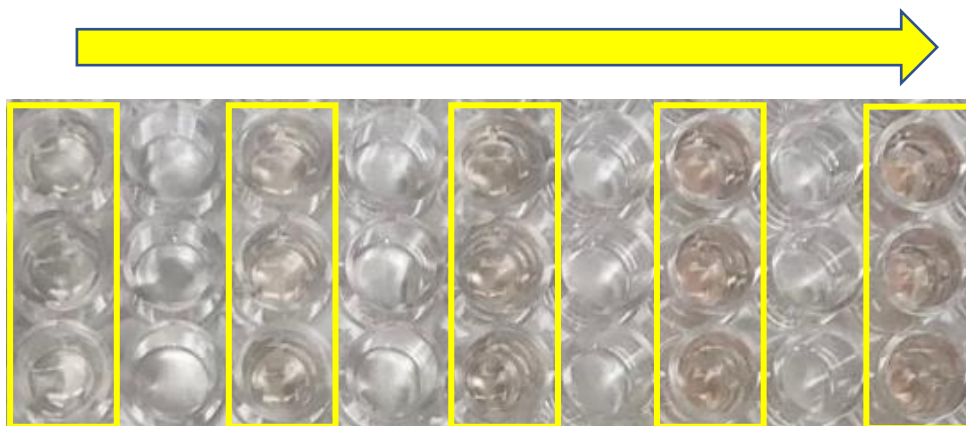


Figure 2.1. Visualization of different extent of tyrosinase inhibition using KA with an increasing concentration gradient. Boxed in yellow are the wells containing reactions (in triplicates). Lighter colors indicate lower tyrosinase activity/ higher inhibition, while stronger pinkish colors indicate higher tyrosinase activity/ lower inhibition.

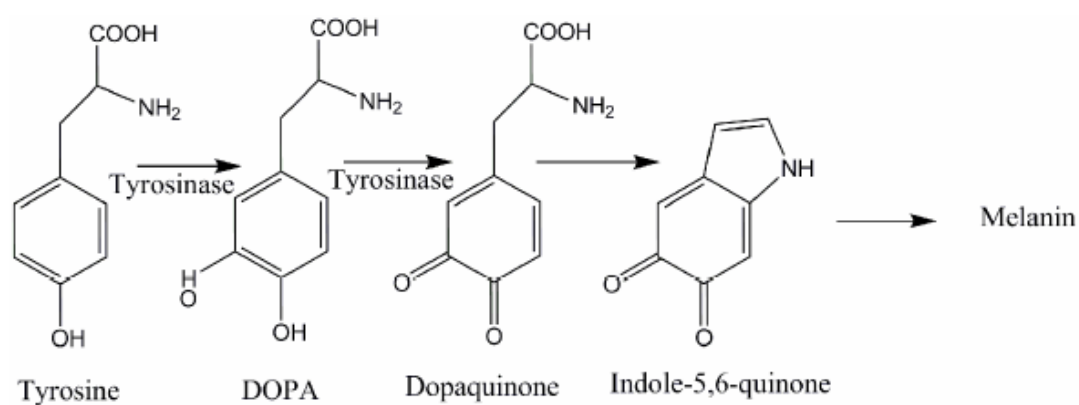


Figure 2.2. Simplified melanin biosynthesis pathway with tyrosinase catalyzing two of the early steps.

II. Materials and Methods

2.1 CYANOBACTERIAL/ALGAL MATERIALS AND REAGENTS

Most of the compounds/fractions used in this Medium Throughput Anti-tyrosinase Screening were purified from various tropical cyanobacterial/algal sample collections made by the Gerwick laboratory during past expeditions. Additionally, some of the compounds from the Gerwick laboratory Pure Compound Library were synthesized by former MS/PhD students or postdoctoral researchers. All samples were stored in DMSO at various concentrations (1/5/10 mg/mL) at -80°C in before dilution and testing.

Mushroom tyrosinase (polyphenol oxidase) was obtained from Sigma Aldrich and Worthington Biochemical Corp. The substrate 3-(3,4-Dihydroxyphenyl)-L-alanine (L-DOPA) was from Tokyo Chemical Industry Corp. Sodium Phosphate buffer (0.1 M, pH6.8) was from bioWORLD Corp. and Kojic Acid (KA) was purchased from Thermo Fisher Scientific Corporation as the positive control (PC). DMSO from Sigma Aldrich was used in small amounts to dissolve samples as well as in controls for consistency with assay procedure.

2.2 REAGENTS PREPARATION

The 0.1 M, pH 6.8 sodium phosphate buffer was diluted with MiliQ Water to a new concentration at 0.067 M to match literature procedures (Masuda *et al.*, 2005). The pH was re-certified using pH paper after each round of buffer preparation. Tyrosinase enzyme was dissolved into diluted buffer and prepared as a 10,000 Units/mL stock solution, and then aliquoted and stored at -20°C until use. For use the 10,000 Units/mL stock solution was diluted to 100 Units/mL with the prepared sodium phosphate buffer described above. All aliquots were used within 2 weeks after preparation to avoid significant loss of activity. One Unit of activity is defined by the manufacturer as causing an increase in the absorbance at

280 nm of 0.001 absorbance units per minute at 25 °C, pH 6.5, using L-tyrosine as the substrate.

2.3 COLORIMETRIC ASSAY FOR BROAD SCREENING

Tyrosinase inhibitory activity of the fractions or pure compounds was evaluated using L-DOPA as the substrate. Experiments were constructed in the format of 96-well microplates (Figure 2.3) for convenience and efficiency, with slight modifications made from previously described method (Masuda *et al.* 2005).

	1	2	3	4	5	6	7	8	9	10	11	12
Sample w/ E	C1	C2	C3	C4	C5	C6	C7	C8	C9	C10	C11	C*
	C1	C2	C3	C4	C5	C6	C7	C8	C9	C10	C11	C**
Sample w/o E	D1	D2	D3	D4	D5	D6	D7	D8	D9	D10	D11	A
	D1	D2	D3	D4	D5	D6	D7	D8	D9	D10	D11	A
Sample w/ E	C12	C13	C14	C15	C16	C17	C18	C19	C20	C21	C22	D*
	C12	C13	C14	C15	C16	C17	C18	C19	C20	C21	C22	D**
Sample w/o E	D12	D13	D14	D15	D16	D17	D18	D19	D20	D21	D22	B
	D12	D13	D14	D15	D16	D17	D18	D19	D20	D21	D22	B

Figure 2.3. Layout of the colorimetric assay for screening for tyrosinase inhibition using 96-well microplates. Samples other than controls were run in triplicates. Four types of wells are shown above: A (Negative control with tyrosinase), B (Negative control without tyrosinase), C (Sample with tyrosinase, 3 wells as replicates), and D (Sample without tyrosinase = sample negative control), respectively. Wells C1-C22 and D1-D22 contained compounds to be tested, while C*, C** and D*, D** contained the known inhibitor kojic acid which served as a positive inhibitor control, run in duplicate.

Briefly, for any individual 96-well plate with samples from our library, all 88 (8 rows x 11 columns) fractions/compounds to be tested were split into four 96-well microplates (22 compounds per plate), to make sure there was space to include duplicates and as a way of minimizing errors. Moreover, for reference and comparison, each plate always included the positive inhibitor control, kojic Acid (KA) (Figure 2.4), a well-known tyrosinase inhibitor (Chang, 2009). This was to ensure that assay conditions (substrate concentrations, incubation time, etc.) were consistent across different assay plates such that the results were comparable.

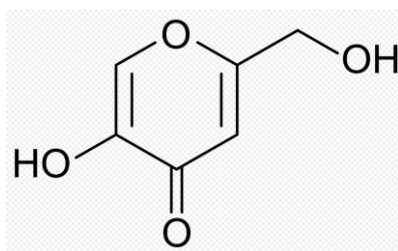


Figure 2.4. Chemical structure of kojic acid (KA), the positive control used in the tyrosinase inhibitory assay.

Four types of assay wells were designated for each screening plate (Figure 2.2), in which the following reaction mixtures were added: **A:** 2 μL of DMSO (solvent control), 118 μL of prepared 0.067 M sodium phosphate buffer and 40 μL of tyrosinase (100 Units/mL) in the same buffer; **B:** 2 μL of DMSO (solvent control) and 158 μL of buffer; **C:** 2 μL of sample (1 mg/mL in DMSO), 118 μL of 0.067 M sodium phosphate buffer and 40 μL of tyrosinase (100 Units/mL) in the same buffer; **D:** 2 μL of sample (1 mg/mL in DMSO) and 158 μL of buffer.

The contents of each well were first mixed and pre-incubated at room temperature for 20 minutes. Then, 40 μL of 3 mM L-DOPA was added as substrate to the reaction mixture, bringing the volume of each well to 200 μL . The final test sample concentration was 10 $\mu\text{g/mL}$, while the final DMSO concentrations for both negative controls and samples were always $\leq 1\%$.

Twenty minutes after addition of the L-DOPA, the plate was read on a SpectraMax M3 plate reader (Molecular Devices, San Jose, CA, USA) for absorbance measurement of each well at 475 nm (for actual calculation) and 490 nm (as a wavelength duplicate) in the endpoint mode. Forty-five seconds of shaking was performed by the instrument before the wells were read.

The percentage inhibition of the tyrosinase activity was calculated by the equation: % Inhibition = $\{[(A - B) - (C - D)] / (A - B)\} \times 100$, where A, B, C & D are all OD values from the corresponding wells at the same time point.

2.4 DOSE-DEPENDENT ASSAY

After the initial broad screening, those samples passing a pre-set threshold of 20% inhibition were considered to be “of further interest”. These more active samples were then evaluated in a dose-dependent assay to detect their tyrosinase inhibitory activity at various concentrations, as well as to re-confirm the activity and filter out any false-positive candidates.

The same 200 μ L reagent mixture system used in the broad screening was also applied in these dose-dependent assays. The only difference was that the concentration of the test sample was varied within the 2 μ L of sample that was added to each well (i.e. 2 mg/mL, 1 mg/mL, 0.5 mg/mL, 0.25 mg/mL and 0.1 mg/mL in DMSO).

For OD measurements, the plate was read using the M3 instrument at 475 nm and 490 nm once L-DOPA was added. The dynamic mode was used where the OD measurements were recorded every minute for 20 minutes. Similarly, 45 seconds of shaking was performed by the instrument before the wells were read.

III. Results and Discussion

Assay validation with KA

Before the formal screening of natural product samples, several test trials were performed using the positive control kojic acid so as to validate the experimental design and evaluate the performance of the tyrosinase, the L-Dopa substrate as well as the KA positive control. The validating experiments used the same experimental setup as for the dose-dependent assay experiments. KA was added at various concentrations to the corresponding

wells. After raw data processing, the inhibitory activity of KA at various concentrations (see Table 2.1) was compared to literature values from preceding studies (Neeley *et al.*, 2009), with data points fit onto a logarithmic curve (see Figure 2.5, $IC_{50} = 5.3787 \mu\text{g/mL} = 37.85 \mu\text{M}$). These experiments established that the protocol was working properly, and thus formal screening of natural product samples could proceed.

Table 2.1. Percent inhibition by kojic acid at various final concentrations. These results were calculated using OD measurements taken after 20 minutes of L-DOPA substrate addition.

Concentration, $\mu\text{g/ml}$	%Inhibition
20	82.2 ± 1.1
10	62.2 ± 2.4
5	49.4 ± 0.4
2.5	28.9 ± 1.7
1	10.3 ± 1.1

Broad Screening

For the broad screening campaign, a total of 2,450 crude material/fractions and all 169 pure compounds in the Gerwick Compound library were tested in the assay. For the samples from the extract library, ‘1550Crude’ to ‘1622I’ were screened to be negative; ‘1623Crude’ was positive; ‘1623A’ to ‘1702Crude’ were negative; ‘1702A’ was positive; ‘1702B’ to ‘A1769B’ were negative; ‘A1769C’ was positive; ‘A1769D’ to ‘A1772B’ were negative; ‘A1772C’ was positive; ‘A1772D’ to ‘1872Crude’ were negative; ‘1872A’ was positive; ‘1872B’ to ‘1982I’ were negative. For the samples from the pure compound library, ‘Ger-1’ to ‘Ger-86’ were negative; ‘Ger-87’ (Scytonemin Monomer) was the only positive, and ‘Ger-88’ to ‘Ger-169’ were again negative. Consequently, among all the samples, only 6 of them passed our pre-set threshold of 20% inhibition and were therefore the best candidates; KA control on the other hand showed >80% inhibition at $10 \mu\text{g/mL}$ (see Figure 2.6). Of the 6 active candidates, 5 samples were for crude extracts or fractions, but they only

barely passed the 20% inhibition threshold at 10 $\mu\text{g/mL}$. The only pure compound showing activity was scytonemin monomer; however, it showed a relatively better inhibition level of ~45% at a screening dose of 10 $\mu\text{g/mL}$, and thus stood out from all others and became our compound of primary interest.

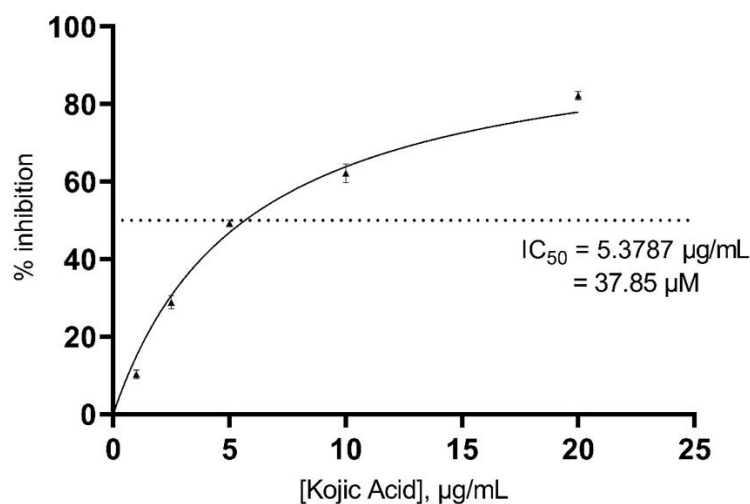


Figure 2.5. Tyrosinase inhibitory activity of KA in a dose-dependent manner. KA was tested at 1 $\mu\text{g/mL}$, 2.5 $\mu\text{g/mL}$, 5 $\mu\text{g/mL}$, 10 $\mu\text{g/mL}$, and 20 $\mu\text{g/mL}$, which was fit by a predicted logarithmic curve. The dotted line represents the IC_{50} value, 5.38 $\mu\text{g/mL}$, which is equivalent to 37.85 μM .

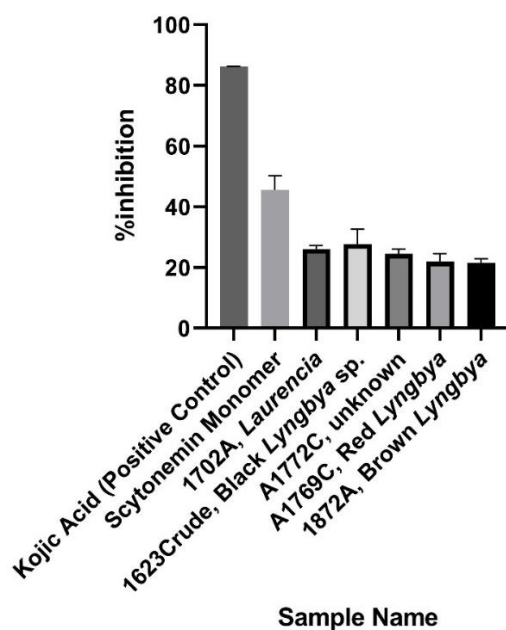


Figure 2.6. Tyrosinase inhibitory activity of the best candidates from the broad screening at 10 $\mu\text{g/mL}$.

Figures 2.7A and 2.7B illustrate the measured absorbance change within 20 minutes for the reagent mixture when no inhibitor was added. The increase in OD reading from ~0.055 to ~0.100 in 2.7A suggested that by the enzymatic addition of tyrosinase, there was a reasonable rate of conversion from L-DOPA to dopaquinone. This agreed with previously known knowledge that dopaquinone is more detectable than L-DOPA at the two wavelengths used in this assay (Behbahani *et al.*, 1993). On the other hand, 2.7B shows a minor or no change in OD, which confirmed the negative control without enzyme addition. However, once the positive control KA or scytonemin monomer (ScyM) was introduced into the reaction, the formation of dopaquinone was retarded, and the OD readings were therefore reduced to a level below 0.100, being ~0.050 and ~0.080, respectively (Figure 2.7C and 2.7E). The negative control experiments for these two inhibitors showed that without enzyme, the OD values were stable across the time period and were consistent with the values for the Blank control (Figure 2.7B, 2.7D and 2.7F). In comparison with the controls, the OD changes observed with the inhibitors KA or ScyM were significant and thus due to a specific inhibition of the enzyme rather than being due to other random factors.

It is important to note in this general screening section that the final concentration of samples and controls were all at 10 $\mu\text{g/mL}$. This reveals that the inhibitory performance of KA and ScyM are different when one takes into account their molar weight difference. The molar inhibitory power of the two compounds will be compared in next chapter, which focuses on the inhibition of tyrosinase by scytonemin monomer.

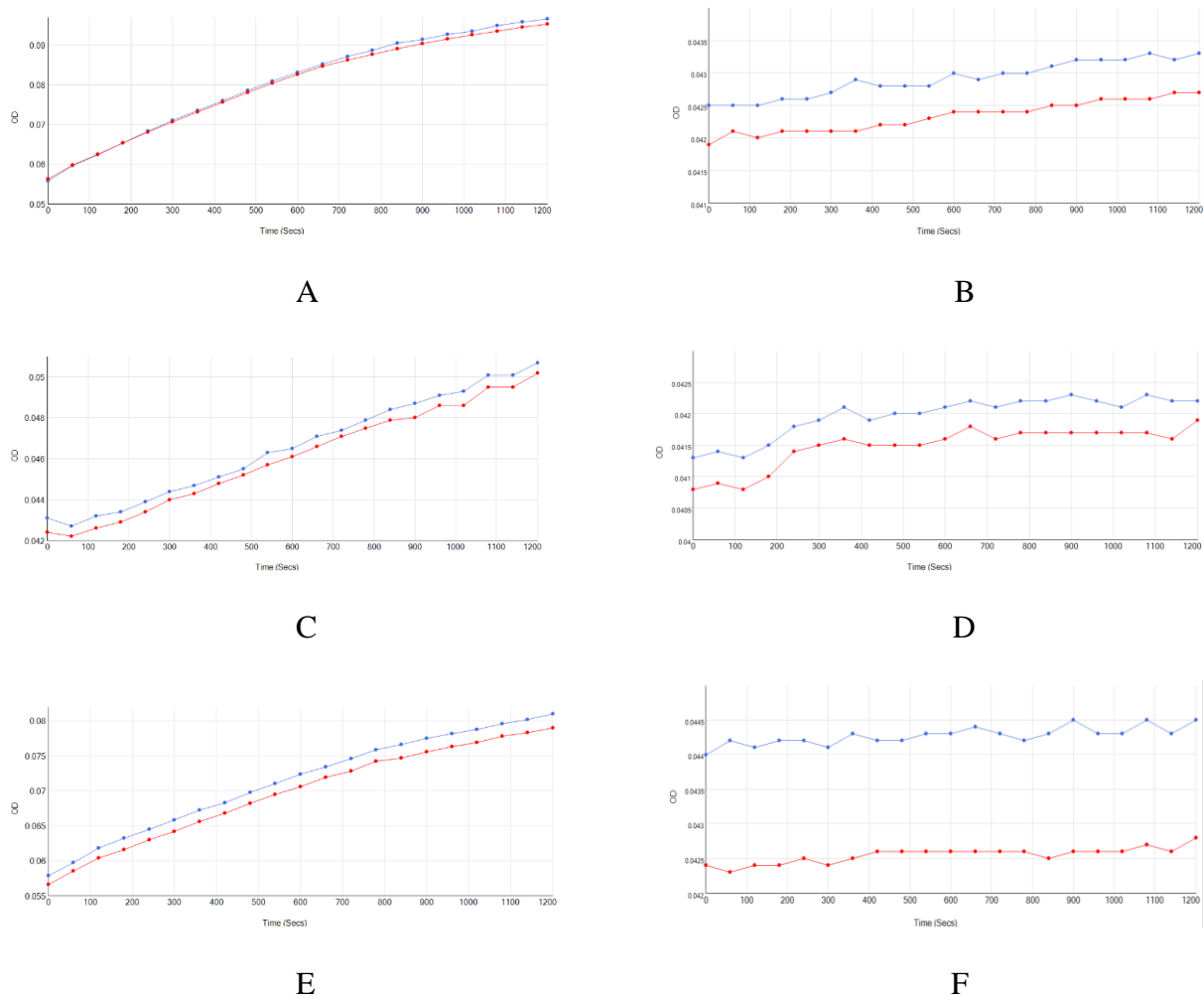


Figure 2.7. Temporal shift of OD readings for: (A) blank with tyrosinase enzyme, (B) blank without enzyme, (C) KA with enzyme, (D) KA without enzyme, (E) ScyM with enzyme, and (F) ScyM without enzyme. Blue lines and red lines represent absorbance values at 475 and 490 nm, respectively.

Dose-dependent Assay

All six active materials from the screening effort were then evaluated in the dose-dependent assay for further analysis. During the timeframe of the OD measurement, only the scytonemin monomer showed reasonable response curves upon varying the sample concentration; this is explored in greater detail in the next chapter.

Unfortunately, all five of the other extract or fraction samples lost their >20% inhibition activity at all concentrations subsequently evaluated. With these multiple results over a series of concentrations, it was clear that the previous results for these five samples were false positives, and therefore should not be further pursued. These results reinforced why we set the preliminary threshold in the broad screening to be >20%, as any inhibition score below 20% might have an even larger chance to be a false positive. The most likely reasons for these false positives may include the fact that strong pigment absorptions hindered accurate OD readings, the time difference between when the reaction took place to the OD measurement, and a loss of tyrosinase activity due to storage of aliquots in the refrigerator.

On the other hand, scytonemin monomer is also a colored material and was thus potentially prone to pigment interference in the assay; however, our multiple re-tests of this material all showed that it retained >20% inhibition, indicating that this was a real result and not coming from a pigment-induced chance error. Furthermore, the stable OD of ScyM without tyrosinase (See the negative controls, Figure 2.7B & 2.7F) also indicated that the >20% inhibition in the complete assay was not due to a pigment effect. Based on our experiences from previous screenings of other colored materials, pigment hinderance could cause substantial changes in the OD readings even in negative controls in which the tyrosinase was not added. But in this case, for the negative control of scytonemin monomer during broad screening (Figure 2.7F) and later tests, the OD values stayed close to the negative control for the blank condition without inhibitor (Figure 2.7B). This result further supported that pigment hinderance had little to no effect in these assays of scytonemin monomer's inhibition of tyrosinase.

IV. Conclusion

Using a validated colorimetric assay to screen for potential tyrosinase inhibitors within samples of the Gerwick Laboratory compound library, we were able to identify six samples that passed the pre-set threshold of 20% inhibition in the general broad screening. After the use of dose-dependent assays to recognize and exclude any false positive results, the pure compound scytonemin monomer showed persistent good inhibition scores, and was thus determined to be a good candidate for further evaluation as a tyrosinase inhibitor. Scytonemin monomer was therefore advanced into the next stage of evaluation, as described in Chapter 3.

References

- Ai N, Welsh WJ, Santhanam U, Hu H, Lyga J. (2014) Novel virtual screening approach for the discovery of human tyrosinase inhibitors. *PLoS One*. 9(11): e112788.
- Behbahani I, Miller SA, Okeeffe DH. (1993) A comparison of mushroom tyrosinase dopaquinone and dopachrome assays using diode-array spectrophotometry: Dopachrome formation vs ascorbate-linked dopaquinone reduction. *Microchem J*. 47(1–2):251–260.
- Chang T-S. (2009) An updated review of tyrosinase inhibitors. *Int J Mol Sci*. 10(6):2440–2475.
- Ha YM, Chung SW, Song S, Lee H, Suh H, Chung HY. (2007) 4-(6-Hydroxy-2-naphthyl)-1,3-benzendiol: a potent, new tyrosinase inhibitor. *Biol Pharm Bull*. 30(9):1711–1715.
- Lima LL, Lima RM, da Silva AF, do Carmo AMR, da Silva AD, Raposo NRB. (2013) Azastilbene analogs as tyrosinase inhibitors: new molecules with depigmenting potential. *ScientificWorldJournal*. 2013:274643.
- Masuda T, Yamashita D, Takeda Y, Yonemori S. (2005) Screening for tyrosinase inhibitors among extracts of seashore plants and identification of potent inhibitors from *Garcinia subelliptica*. *Biosci Biotechnol Biochem*. 69(1):197–201.
- Mutschlechner B, Rainer B, Schwaiger S, Stuppner H. (2018) Tyrosinase Inhibitors from the Aerial Parts of *Wulfenia carinthiaca* Jacq. *Chem Biodivers*. 15(4):e1800014.
- Neeley E, Fritch G, Fuller A, Wolfe J, Wright J, Flurkey W. (2009) Variations in IC(50) values with purity of mushroom tyrosinase. *Int J Mol Sci*. 10(9):3811–3823
- Yang HH, Oh K-E, Jo YH, Ahn JH, Liu Q, Turk A, Jang JY, Hwang BY, Lee KY, Lee MK. (2018) Characterization of tyrosinase inhibitory constituents from the aerial parts of *Humulus japonicus* using LC-MS/MS coupled online assay. *Bioorg Med Chem*. 26(2):509–515.
- Zolghadri S, Bahrami A, Hassan Khan MT, Munoz-Munoz J, Garcia-Molina F, Garcia-Canovas F, Saboury AA. (2019) A comprehensive review on tyrosinase inhibitors. *J Enzyme Inhib Med Chem*. 34(1):279–309.

CHAPTER THREE

SCYTONEMIN MONOMER (ScyM) CASE STUDY: EXAMINING THE INHIBITORY POTENTIAL AND INHIBITION MODE OF SCYTONEMIN MONOMER AGAINST TYROSINASE ENZYME

Abstract

The proposed biosynthetic pathway of scytonemin, a well-known cyanobacterial sunscreen, ends with the dimerization of two scytonemin monomer (ScyM) units as the final step. While preliminary study in Chapter two disclosed the tyrosinase inhibitory potential of ScyM for the first time, via further analysis detailed in this Chapter, the inhibitory mode and efficacy of ScyM were determined. The re-synthesized crude ScyM was purified through HPLC and checked with LCMS and NMR to validate its identity and purity. The purified ScyM was tested in multiple dose-dependent tyrosinase inhibition assays, through which the half maximal inhibitory concentration (IC_{50}) of ScyM was determined. The IC_{50} of ScyM was $4.90 \mu\text{M}$, while that of the positive control kojic acid (KA) was $11.31 \mu\text{M}$, indicating that ScyM is more potent in inhibiting tyrosinase than the commercially available standard inhibitor KA. Through kinetic mode analysis, the Lineweaver-Burk plots were generated to determine the inhibition parameters and its mixed-type mode of inhibition. For enhanced visualization, a 3D overview of ScyM inside the tyrosinase binding pocket was generated through molecular docking, which revealed both the potential of ScyM to function as a copper chelator inhibitor, and the importance of the phenol moiety of ScyM for its critical role played in tyrosinase inhibition. Interestingly, the dimeric compound scytonemin lost these unique bioactivities of ScyM (anti-tyrosinase and antioxidant properties), while both compounds were found to be non-cytotoxic to mammalian cells.

I. Introduction

As one of the most crucial resources on earth, sunlight supports life which results in biologically available carbon and oxygenation of the atmosphere (Mathews, *et al.*, 2000). But at the same time, the sun also emits ultraviolet (UV) radiation at shorter wavelengths. This UV radiation has higher energy and may cause significant damage to DNA for both animals and plants, which in turn affects proper cell growth and development and eventually leads to multiple kinds of diseases (Roy, 2017). To avoid these UV-induced negative effects, many organisms have evolved the ability to biosynthesize various UV-absorbing metabolites as a defense against UV radiation.

Scytonemin, the pigment material found in the sheaths of many species of cyanobacteria, is such an example of a UV-absorbing molecule and is often referred as “cyanobacterial sunscreen pigment” due to this property (Proteau *et al.*, 1993). It is also considered as a biogeochemical marker as a result of its stable nature and “recalcitrancy to degradation” (Garcia-Pichel and Castenholz, 1991). Although its existence was discovered early in the 19th century (Nägeli, 1849), because of its complex structure, the dimeric indole phenolic skeleton of scytonemin was not elucidated until 1993 by the Gerwick group. This newly found skeletal type is composed of both indolic and phenolic subunits and was named the “scytoneman skeleton” (Proteau *et al.*, 1993).

Motivated by its unique and complex structure, study of the biosynthesis of scytonemin was of great interest and conducted at both the genomic and mechanistic level in several research laboratories. In 2007, for the first time the molecular genetics of scytonemin biosynthesis was explored by Soule *et al.*, using a transposon mutagenesis approach in the cyanobacterium *N. punctiforme*. After two more years studying on this topic, an 18-gene cluster (NpR1276 to NpR1259) was successfully identified to be associated with scytonemin biosynthesis (Soule, Palmer, *et al.*, 2009). In the same year,

research by Sorrels *et al.* further helped describe the cluster boundaries and revealed the correlation between biosynthetic cluster regulation and UV radiation. Additionally, through phylogenetic analyses, the presence of the scytonemin biosynthetic gene cluster across several cyanobacterial lineages was found, and a potential ancient evolutionary origin for scytonemin gene cluster was proposed (Sorrels *et al.*, 2009). Furthermore, an upstream two-component regulatory system (NpF1277 and NpF1278) was discovered and shown to regulate the expression of the main 18-gene scytonemin cluster, while another set of 5 satellite genes (NpF5232 to NpF5236) was also considered to be involved in scytonemin biosynthesis (Soule, Garcia-Pichel, *et al.*, 2009; Janssen and Soule, 2016). These satellite genes were referred as *ebo* genes in a recent study, in which the *ebo* genes were proven to be responsible for the export of the final precursor from the cytoplasm to the periplasm, the location where the final steps of scytonemin biosynthesis takes place (Klicki *et al.*, 2018).

Another breakthrough on scytonemin biosynthesis was made when Balskus and Walsh proposed a mechanism for the biosynthetic pathway in which the characterization of biosynthetic enzymes could related to this genetic work. This biosynthesis was proposed to start with two aromatic amino acids, tryptophan and tyrosine, to form two indole-3-pyruvic acid (IPA) and *p*-hydroxyphenylpyruvic acid (HPP) precursors, which are responsible for the conjugated skeleton of scytonemin upon condensation (Balskus and Walsh, 2008). Using small-scale isotope labeling technique, this idea was further validated with *in vivo* data (Jones *et al.*, 2011). And two enzymes/putative enzymes encoded in the identified 18-gene cluster of scytonemin, namely ScyB (NpR1275) and TyrA (NpR1269), were found to be involved in the formation of the pyruvic acid derivatives (Balskus and Walsh, 2009; Gao and Garcia-Pichel, 2011). Subsequently, another enzyme ScyA (NpR1276) was shown to catalyze the acyloin coupling of the IPA and HPP precursors to bind the two subunits together (Balskus and Walsh, 2008). After that, one more enzyme encoded in the scytonemin gene

cluster, ScyC (NpR1274), was found to catalyze cyclization and decarboxylation to form a ketone that could further undergo oxidation to form the scytonemin monomer (Balskus and Walsh, 2009). As the last step in this pathway, scytonemin monomer was thought to form scytonemin through oxidative dimerization. Although speculated to be the tyrosinase encoded by *trpA* (Npr1263) (Balskus and Walsh, 2008; Sorrels *et al.*, 2009), the actual clear information on the enzyme responsible for catalyzing this coupling reaction of two monomers is still missing. On the other hand, while ScyE was proven to be crucial for scytonemin biosynthesis, its exact role remains ambiguous; ScyD and ScyF are not essential for the last steps of scytonemin biosynthesis and might be redundant genes (Ferreira and Garcia-Pichel, 2016). However, a clear mechanism for this last dimerization step is still undetermined. Additionally, the signaling pathway(s) and the sensing of abiotic stressors that upregulate scytonemin biosynthesis is not yet described (Pathak *et al.*, 2020). A most comprehensive model based on all previous research on scytonemin biosynthesis is shown in Figure 3.1.

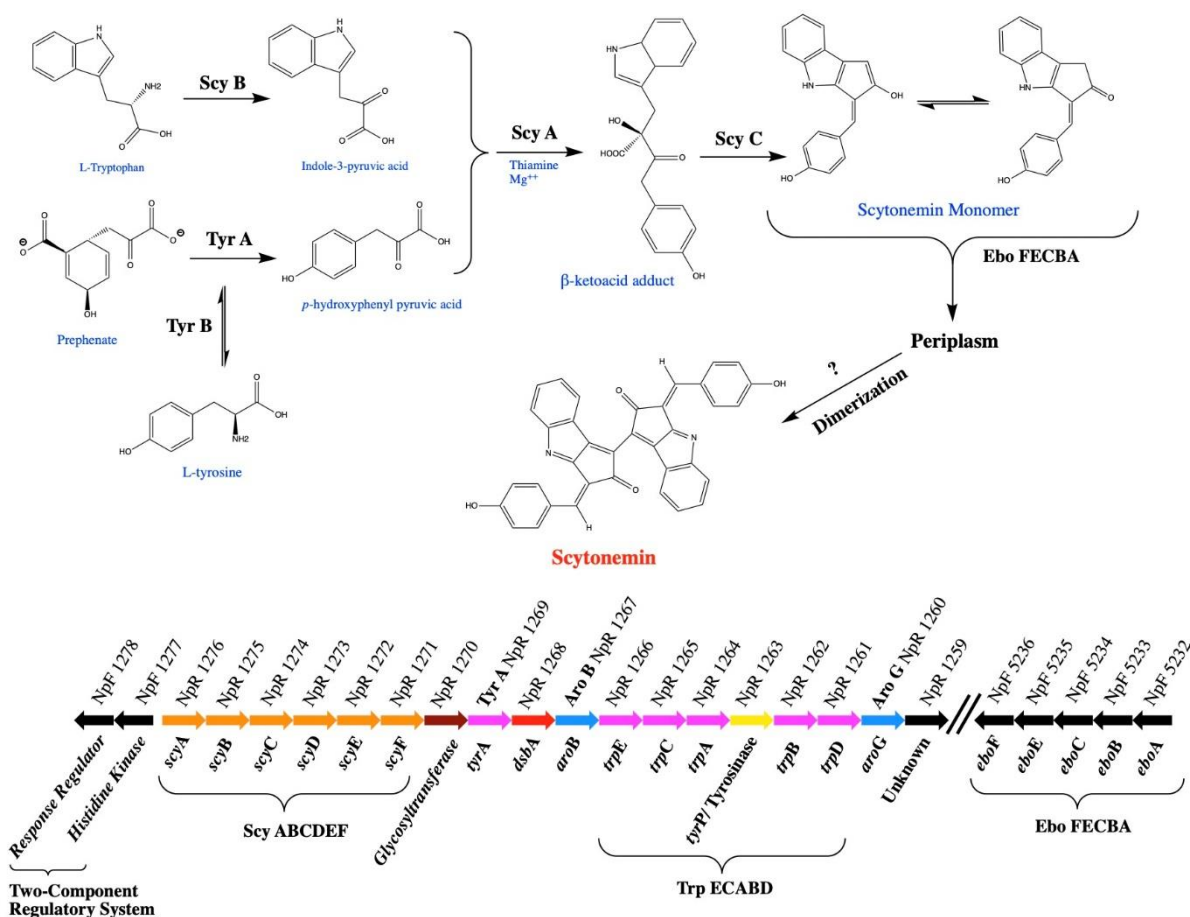


Figure 3.1. A diagram showing the biosynthesis pathway of scytonemin in *Nostoc punctiforme* ATCC 29133 and corresponding gene products involved in the biochemical steps. Arrows within gene cluster shows the direction of transcription. The main 18-gene cluster (NpR1276 to NpR1259) contains *scyA*, *scyB*, *scyC*, and *tyrA*, which encode the four key intermediate-forming enzymes, ScyA, ScyB, ScyC, and TyrA, respectively. Genes represented by the magenta arrows were responsible for the formation of pyruvic acid derivatives as precursors of scytonemin. An upstream two-component regulatory system (NpF1277 and NpF1278) regulates the expression of the main 18-gene scytonemin cluster. The set of 5 satellite genes (NpF5232 to NpF5236), referred to as *ebo* genes, encodes the Ebo complex. The Ebo complex exports the final precursor scytonemin monomer from the cytoplasm to the periplasm, where the monomers are dimerized to form the final product scytonemin with the help of mysterious enzyme(s) not yet determined. Figure recreated based on Pathak *et al.*, 2020.

The biological activities of scytonemin have been reported in a number of reports since its discovery. It has been shown to possess anti-inflammatory, anti-tumor and calcium antagonistic properties by different research laboratories (Helms *et al.*, 1988; Stevenson *et al.*, 2002; Itoh *et al.*, 2014), in addition to its UV sunscreen properties (Garcia-Pichel and

Castenholz, 1991). However, there has been limited biological testing of ScyM, the proposed final precursor in the scytonemin biosynthetic pathway. This might be because the total synthesis of scytonemin and sustainable production of scytonemin monomer was only published relatively recently such that access to this material has been fairly restricted for scientists (Ekebergh *et al.*, 2011; Malla and Sommer, 2014).

Through broad screening and subsequent multiple dose-dependent evaluations, the tyrosinase inhibitory activity of scytonemin monomer (See Figure 3.2 for structure) was identified and confirmed as described in Chapter 2, and this may open a new window on the study of the biological properties of this compound. However, all remaining ScyM material was expended, and therefore any additional in-depth analysis was prevented. But fortunately, we were able to connect with Dr. Tak Suyama who first synthesized this compound in Gerwick lab in 2009 and now a professor at Waynesburg University. Dr. Suyama generously offered to re-synthesize more scytonemin monomer (ScyM) and its methoxylated analog (ScyM-OMe) for us, and with these materials I was able to resume the study.

Using this newly synthesized ScyM, this chapter further investigated the tyrosinase inhibitory activity of ScyM by confirming its dose-dependent response and generating a reliable IC_{50} value for comparison with other inhibitors. I also examined the inhibition mode via a kinetic analysis using Lineweaver-Burk plots, and deduced its potential positioning inside the tyrosinase binding site through in-silico docking.

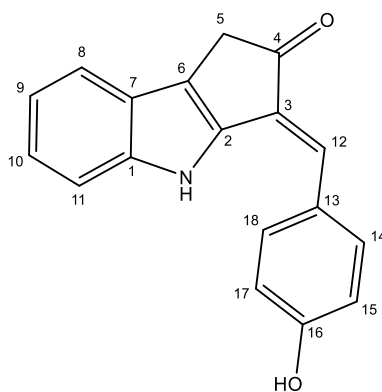


Figure 3.2. Structure of scytonemin monomer (ScyM) used in this study.

II. Materials and Methods

2.1 STRUCTURE ELUCIDATION/VALIDATION AND PURIFICATION OF RE-SYNTHEZED SCYTONEMIN MONOMER (ScyM)

The ScyM was synthesized using a commercially available tricyclic precursor (3,4-dihydrocyclopenta[b]indol-2(1H)-one) and 4-hydroxybenzaldehyde (See Figure 3.3) by Dr. Tak Suyama at Waynesburg University and shipped to Gerwick Lab for use in this study. The 3,4-dihydrocyclopenta[b]indol-2(1H)-one enamine starting material was purchased from Sigma Aldrich. All the LCMS analyses were carried out on a Thermo Finnigan Surveyor Autosampler-Plus/LC-Pump-Plus/PDA-Plus system and a Finnigan LCQ Advantage Plus mass spectrometer, with samples dissolved at 1 mg/mL in MeOH. Reversed-phase HPLC was performed on a Kinetex C18 semipreparative column (100 × 4.6 mm × 5 μm, Phenomenex) using a Thermo Fisher Scientific HPLC system comprising a Thermo Dionex UltiMate 3000 pump, RS autosampler, RS diode array detector, and automated fraction collector. For the RP-HPLC method to purify ScyM, once identified the retention time, an isocratic gradient of 50% acetonitrile in purified H₂O was used to improve the purity of the crude ScyM product. Both acetonitrile and H₂O solvents contained 0.1% (v/v) formic acid.

1D NMR and 2D NMR spectra were acquired using a Bruker Avance III DRX-600 NMR and a JEOL ECZ 500 NMR spectrometer with N, N-dimethyl-formamide-d₇ (DMF-d₇) (Cambridge Isotope Laboratories, Inc.) used as solvent.

Samples were purified with C18 SPE (5000 mg/20 mL, SEClute) before being injected into various instruments for analysis. All other general solvents were HPLC grade as purchased from Thermo Fisher Scientific. A Millipore Milli-Q system (Burlington, MA, USA) was used to purify water.

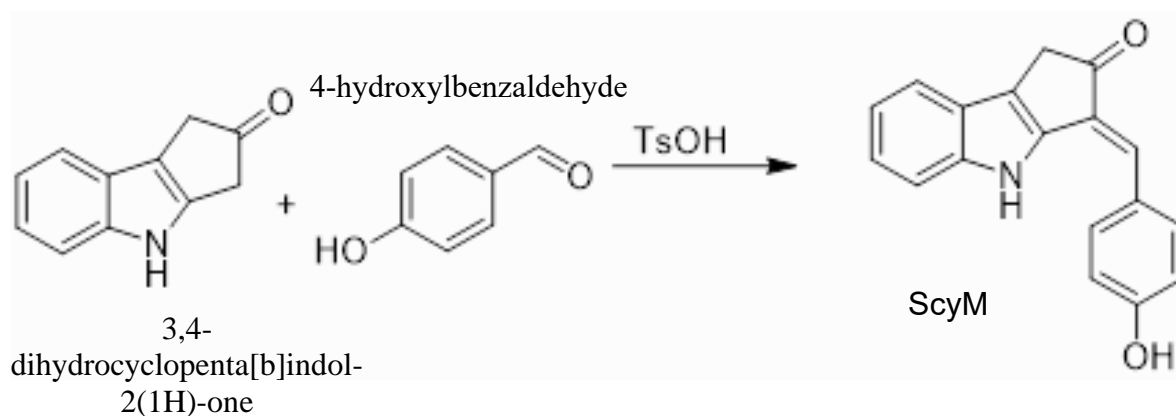


Figure 3.3. Simplified synthetic method to produce ScyM. Commercially available 3,4-dihydrocyclopenta[b]indol-2(1H)-one and 4-hydroxybenzaldehyde were used as starting materials.

2.2 TYROSINASE INHIBITION ASSAY

Similar to Chapter two, tyrosinase inhibitory activity of materials was evaluated using L-DOPA as the substrate. Experiments were carried in triplicate in 96-well microplates with the same 200 μL system used in the previous dose-dependent assays. The only difference was that the concentration gradient for the 2 μL of sample (test material or positive control KA) added into wells was set to be 200 μM , 150 μM , 75 μM , 25 μM , 5 μM and 1 μM .

For OD measurements, the plate was read using the SpectraMax M3 plate reader at 475 nm (for actual calculation) and 490 nm (as a wavelength duplicate) in the dynamic mode for 60 minutes with measurements recorded per minute. Forty-five seconds of shaking was performed by the instrument before the wells were read. Percent inhibition was calculated using the same formula as in Chapter 2. The IC_{50} values and curves of average percent inhibition (triplicates) versus sample concentration were generated using data read at 5 min with Graphpad Prism 9.2.0.

2.3 KINETIC ANALYSIS OF TYROSINASE AND INHIBITORS

The mode of inhibition and inhibition parameters, i.e. the Michaelis–Menten constant (K_m) and maximal velocity (V_{max}) of tyrosinase, were determined by Lineweaver–Burk plot analysis using various concentrations of L-DOPA (0.15 mM, 0.3 mM and 0.6 mM) as substrate. To accommodate for solubility, the inhibitor concentrations for ScyM were 10 μ M, 5 μ M, 2.5 μ M, 1.25 μ M and 0 μ M; for KA the concentrations were 25 μ M, 10 μ M, 5 μ M, 2.5 μ M and 0 μ M. The Lineweaver–Burk plot was generated using Graphpad Prism 9.2.0. Experiments were performed in triplicate.

2.4 MOLECULAR DOCKING EXPERIMENT

All docking analyses were carried out using the Molecular Operating Environment 2019 (MOE 2019.0102) program, in which the docking results were manipulated using the GBVI/WSA dG scoring function that estimates the free binding energy of the ligand from a given orientation. Among the various tyrosinase enzyme crystal structures available in the Protein Data Bank, the *A. bisporus* tyrosinase enzyme co-crystallized with built-in tropolone inhibitors (PDB code: 2Y9X) was selected for molecular docking study for consistency, as the mushroom tyrosinase enzyme was used in all of the *in vitro* tyrosinase inhibition assays. 3D structures of L-DOPA, KA, scytonemin, ScyM, and ScyM-OMe were prepared using the Builder module with energy minimization. Docking was performed with 2000 poses once ligands were securely positioned in the enzyme binding pocket, and the best five poses were decided based on the negative binding free energy value (S value) and then selected to analyze receptor-ligand interactions. The cognate ligand inside 2Y9X, tropolone, was re-docked in the pocket as a validation of docking accuracy. Accordingly, a reasonable S value of -5.95 was obtained for the re-docked tropolone, and the resulted binding poses along with

ligand interactions were close to its original reference conformation [root-mean-square deviation (RMSD) = 1.02 Å] (Ismaya *et al.*, 2011).

2.5 CYTOTOXICITY ASSAY

The cytotoxicity assay was performed using a protocol described in previous papers of the Gerwick lab (H-B. Yu *et al.*, 2019; Leber *et al.*, 2020). The MTT staining method was used to determine the cytotoxicities of compounds of interest using the NCI-H460 human lung carcinoma cell line purchased from ATCC (Manassas, VA, USA). The cells were grown in flasks and then seeded into wells at 3.33×10^4 cells/mL of Roswell Park Memorial Institute (RPMI-1640) medium with standard fetal bovine serum (FBS), leading to 180 μ L/well. The cells were subsequently pre-incubated for 24 h at 37 °C in 96-well plates before drug was added. Thereafter, with addition of diluted compounds of interest dissolved in DMSO, plates were incubated for an additional 48 h and then stained with MTT (thiazolyl blue tetrazolium bromide 98%; Sigma-Aldrich) for 25 min, after which the optical densities (OD) were recorded at 630 and 570 nm for each well on a SpectraMax M3 plate reader (Molecular Devices, San Jose, CA, USA). Doxorubicin and 1% DMSO in RPMI-1640 without fetal bovine serum were used as positive and negative controls, respectively. Polyethylene glycol (PEG) was used to facilitate dissolution for compound with solubility issue.

III. Results and Discussion

Structure elucidation/validation and purification of re-synthesized ScyM

Once the re-synthesized crude ScyM material (Figure 3.3) was received from Dr. Tak Suyama, it was directly injected for liquid chromatography and mass spectrometry (LCMS) analysis to check its purity and structure. In the positive mode MS spectrum, ScyM (exact mass = 275.09) showed a parent peak at m/z 275, while the MS² spectrum showed a more detailed pattern for this peak and suggested a potential [M-28] fragmentation pattern (Figure 3.4B & Figure 3.5). This base peak and peak pattern matched perfectly with previously recorded high resolution MS data when ScyM was first time produced, which was also performed in the positive ion mode (Suyama, 2009). The hypothesized [M-28] peak might derive from an unusual loss of C = O that breaks the polycyclic structure during the fragmentation and ionization in the mass spectrometer. While we were not able to get solid experimental proof for this cleavage, such a break of the polycyclic structure together with loss of carbonyl group to result in a [M-28] peak, was also observed for other indole derivatives that highly resemble the structure of ScyM (Rodríguez *et al.*, 1996). These examples from previous mass spectrometry studies provide further support for the possibility of a comparable [M-28] fragmentation pattern for ScyM.

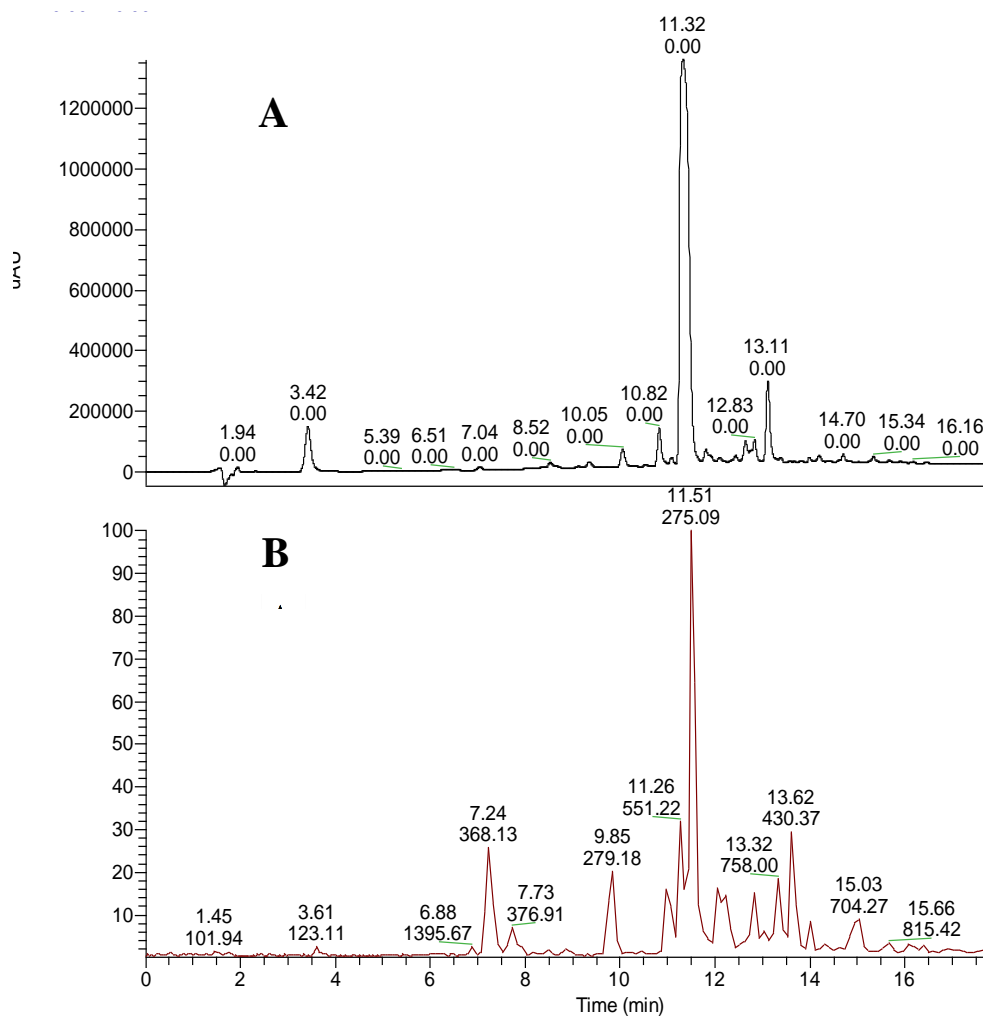


Figure 3.4. Liquid chromatography and mass spectrometry (LCMS) spectra of the crude ScyM product in the positive ionization mode. A) Total PDA detection with the major compound detected at the retention time (RT) of 11.32 min. B) Total ion mass detection with highest ScyM peak m/z 275 showing at RT = 11.51 min.

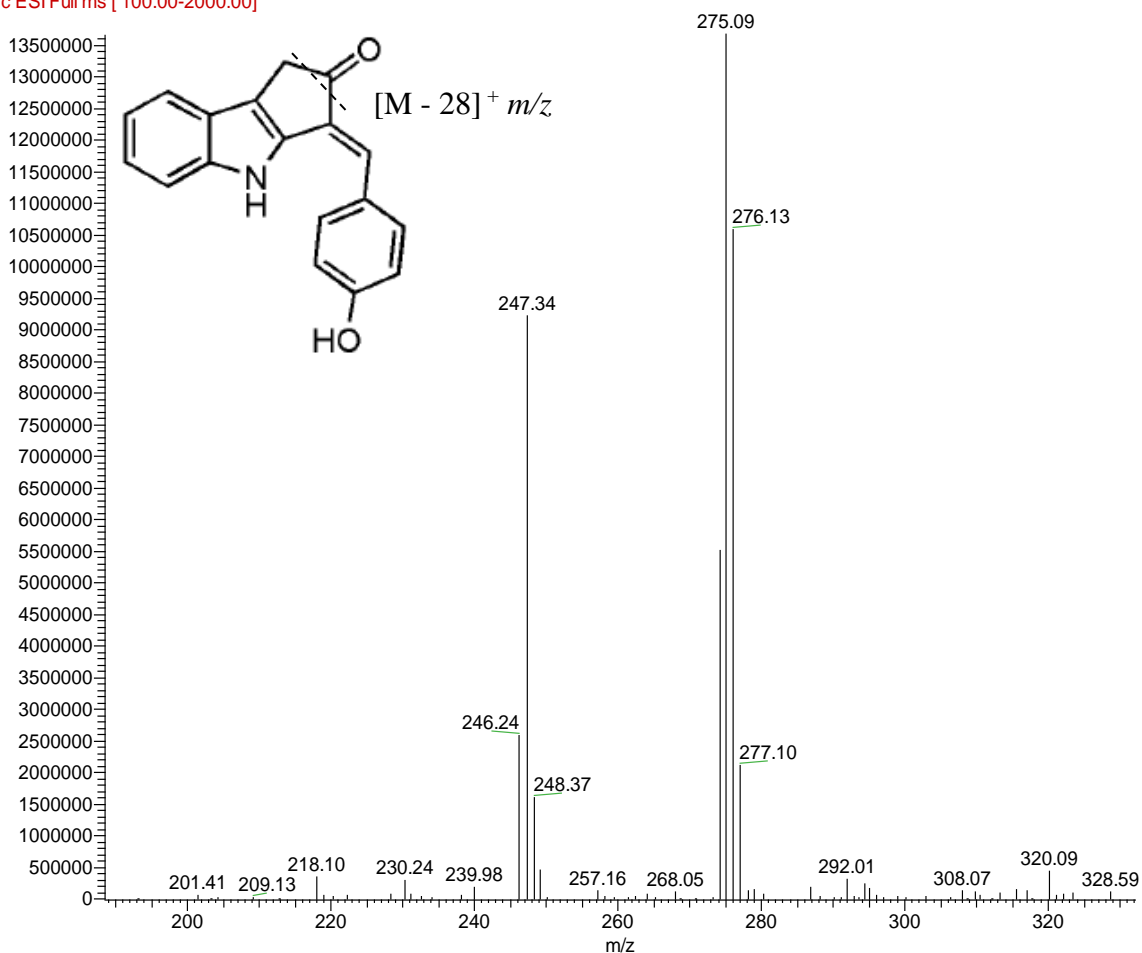


Figure 3.5. MS² spectrum of scytonemin monomer peak in positive mode electrospray ionization (+ESI) with potential fragmentation of [M - 28].

While the MS profile confirmed the existence of ScyM in the crude material, the PDA and mass spectra meanwhile revealed several other peaks (See Figure 3.4A & 3.4B) which were impurities from the synthesis (possibly leftover precursors and (or) byproducts of the synthesis). For example, the m/z 123 peak eluting at RT = 3.61min was recognized to be remaining 4-hydroxybenzaldehyde (See Figure 3.3 for structure) that was used as starting material in ScyM's synthesis. As a result, a further HPLC purification was performed using a portion of crude ScyM (~10 mg) dissolved in MeOH. The ScyM peak was isolated following the protocol described in the Methods section and ~4.4 mg of pure material was retrieved. This purified ScyM was again checked for MS profile and showed a much better purity

profile with a clean m/z 275 peak plus fewer and less intense other peaks (Figure 3.6A & 3.6B), indicating most of the impurities were successfully filtered through HPLC performed. Additionally, the remaining stubborn impurity peaks were much lower in relative abundance according to the MS profile, which again confirmed that there were little disturbing constituents in the sample after HPLC and the ScyM material was of good purity and should be eligible for the tyrosinase inhibition assays.

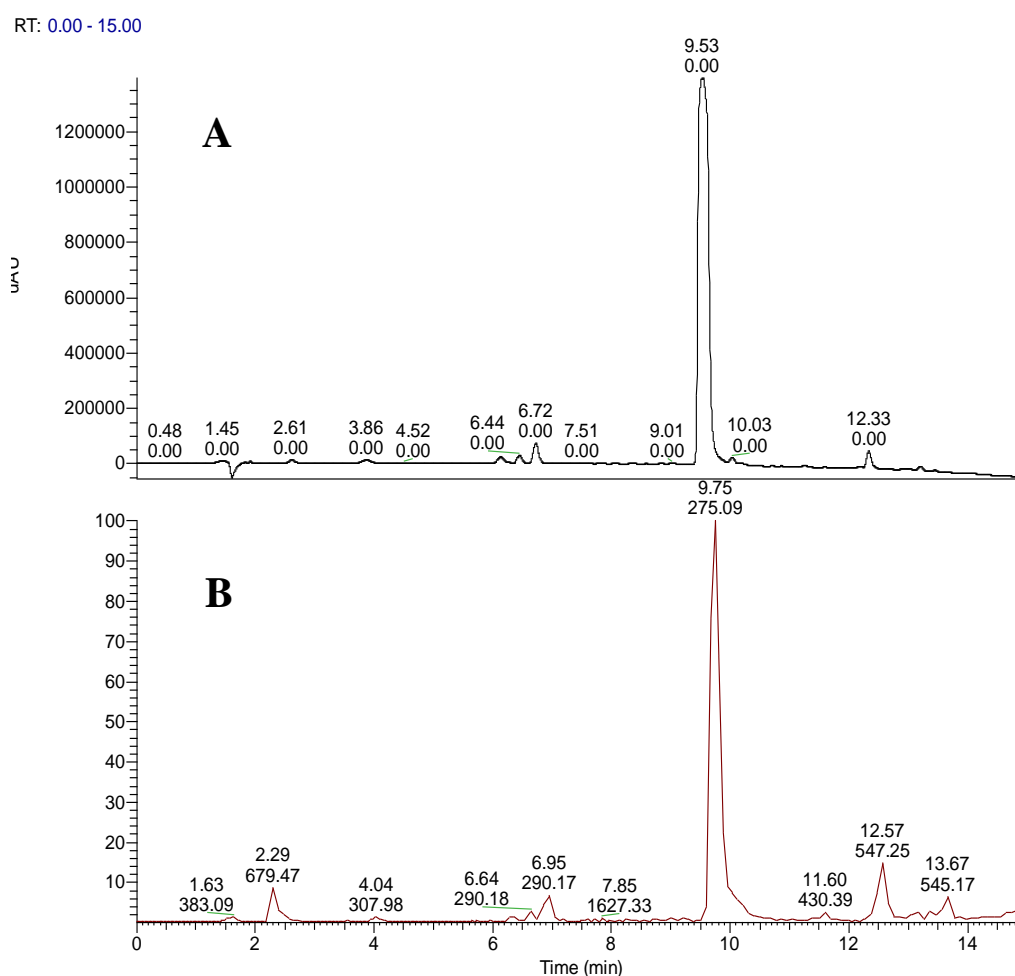


Figure 3.6. LCMS spectra of post-HPLC purified ScyM in the positive ionization mode. A) Total PDA detection with major compound detected at the retention time (RT) of 9.53 min. B) Positive ion ESI MS monitoring of eluted peaks with the isolated ScyM peak m/z 275 showing at RT = 9.75 min. Both traces indicated a much better purity compared with the crude ScyM material.

It was noticed that there was a small discrepancy in the RT for the eluted m/z 275 ScyM peak before and after purification (See Figure 3.4 and 3.6). This was considered to be due to a systemic error/fluctuation from the LCMS instrument, which has experienced inaccuracy and hence re-calibration between the time when the two measurements above were taken. To clear any ambiguity, the crude ScyM was checked again by LCMS and the resulting retention time matched well with that of purified material (See Figure 3.6 and 3.7), proving that it was the same m/z 275 ScyM peak in the spectra before and after purification.

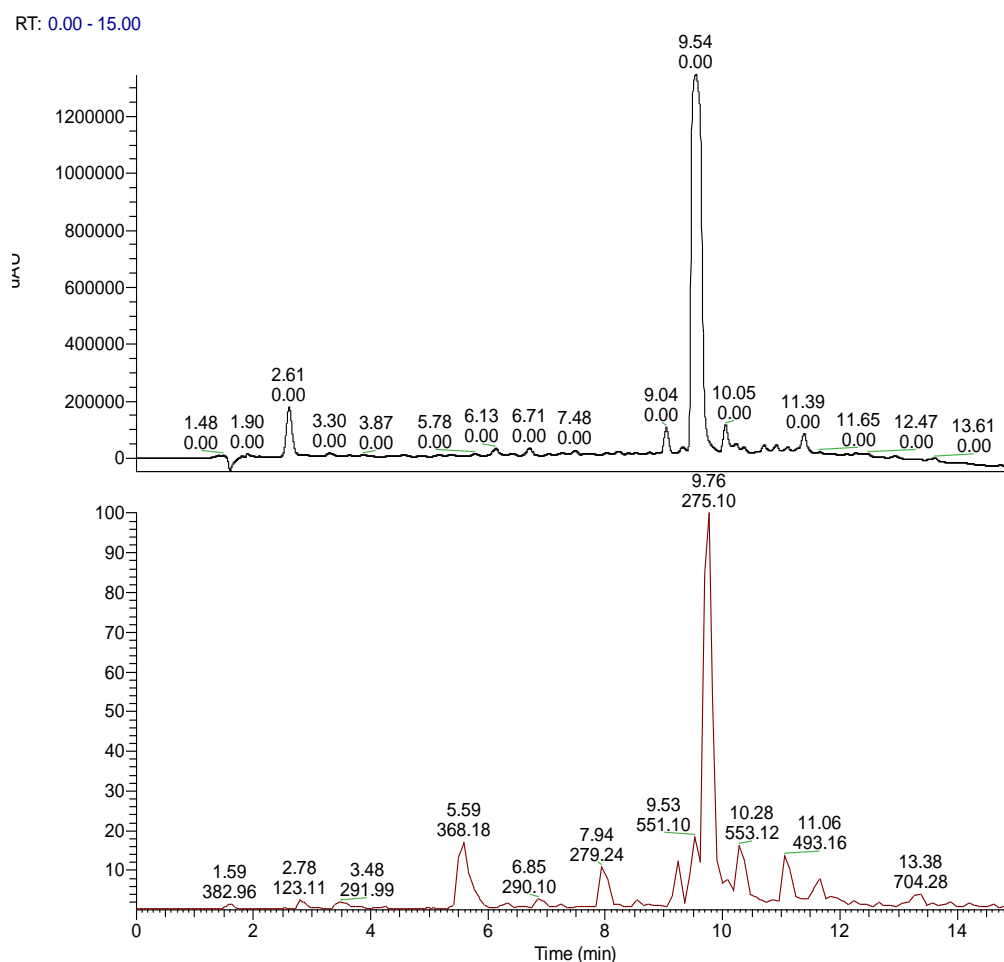


Figure 3.7. Re-check of LCMS analysis of crude ScyM in the positive ionization mode. A) Total PDA detection with the major compound detected at the retention time (RT) of 9.54 min. B) Positive ion ESI MS monitoring of eluted peaks with the isolated ScyM peak m/z 275 showing at RT = 9.76 min. Both LCMS runs demonstrated good consistency with data for scytonemin post-HPLC purification.

The NMR data of ScyM was also obtained as an extra validation for the ScyM structure (See Table 3.1). The same numbering pattern of carbons following Dr. Tak Suyama's work is shown in Figure 3.2. The solvent peaks of DMF-d₇ (¹H: 8.03, 2.92, 2.75; ¹³C: 163.15, 34.89, 29.76) were used as internal chemical shift references. Additionally, 2D NMR spectra, such as HSQC and HMBC, were also performed to help with the assignment of carbon atoms (Figure 3.8). Again, all NMR results corresponded well with previously published data (Suyama, 2009). Conclusively, all the results from LCMS and NMR together confirmed the identity and purity of ScyM.

Table 3.1. Observed and Expected (as reported Suyama, 2009) ¹H and ¹³C NMR Spectroscopic Data of Scytonemin Monomer (ScyM) in DMF-d₇

Position	Observed		Expected	
	δ_C , type	δ_H (J in Hz)	δ_C , type	δ_H (J in Hz)
1	141.44, C		141.6, C	
2	141.25, C		141.4, C	
3	127.07, C		127.3, C	
4	205.26, C		205.3, C	
5	36.76, CH ₂	3.56, s	36.9, CH ₂	3.56, s
6	120.64, C		120.9, C	
7	125.03, C		125.2, C	
8	120.20, CH	7.57, d (7.89)	120.4, CH	7.57, d (8.0)
9	121.08, CH	7.12, ddd (7.54, 7.21, 1.02)	121.2, CH	7.12, ddd (7.9, 4.5, 0.6)
10	124.34, CH	7.23, ddd (8.25, 6.91, 1.22)	124.4, CH	7.23, ddd (8.2, 7.2, 1.3)
11	113.82, CH	7.61, d (8.28)	113.9, CH	7.60, d (8.1)
12	125.36, CH	7.06, s	125.4, CH	7.06, s
13	127.26, C		127.6, C	
14, 18	131.58, CH	7.70, d (8.66)	131.7, CH	7.70, d (8.5)
15, 17	117.42, CH	6.98, d (8.55)	117.3, CH	6.97, dd (6.1, 2.4)
16	160.31, C		160.2, C	

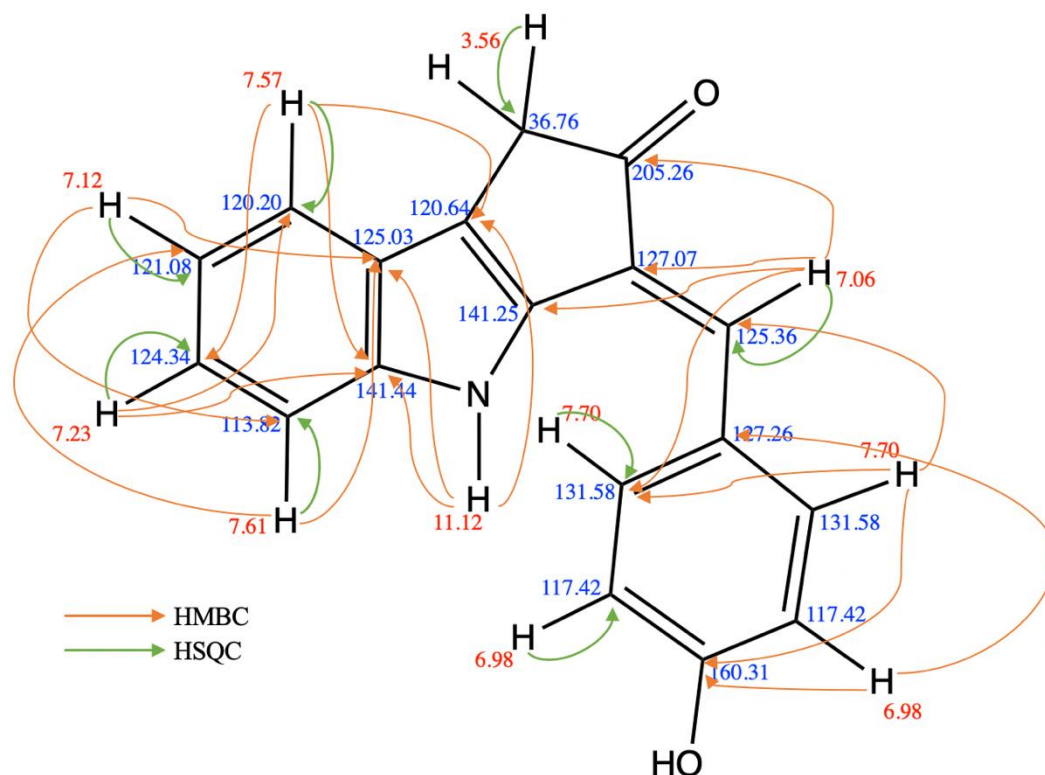


Figure 3.8. HMBC and HSQC correlations for scytonemin monomer in DMF- d_7 . ^1H NMR shifts are shown in red and ^{13}C NMR shifts are shown in blue.

Tyrosinase inhibitory activity of ScyM in comparison with KA

Different from screening in Chapter 2, because the molecular weights of all compounds being evaluated in the tyrosinase assay were known, the final concentrations of the samples were set in μM instead of $\mu\text{g/mL}$ in the new rounds of tyrosinase inhibition assays. In this way, the inhibitory power of different compounds became more accurately comparable as they were in molar concentrations.

As a first check of the inhibitory activity for the newly synthesized ScyM, a dose-dependent assay was performed in kinetic mode for both ScyM and the KA control; newly synthesized but unpurified ScyM was used for this initial confirmation assay. Figure 3.9A and 3.9B provide the results of the calculated time-dependent inhibition of the two compounds.

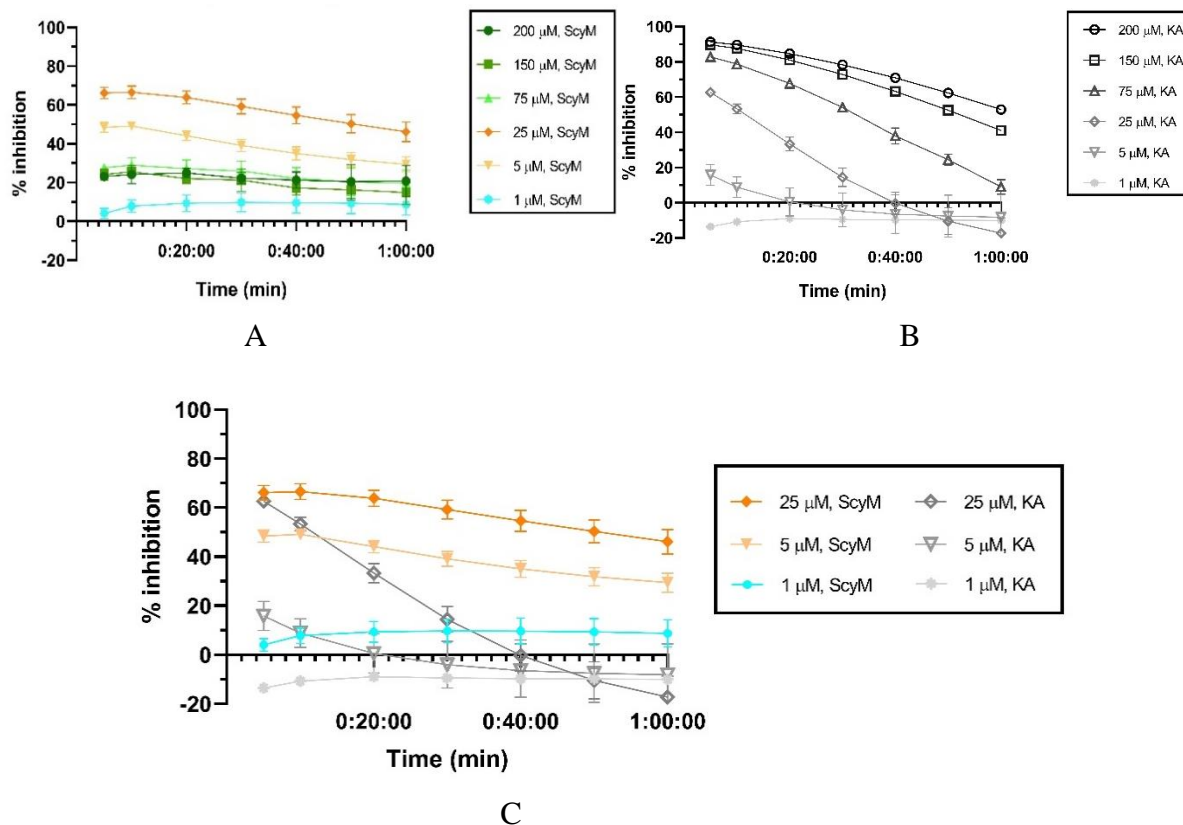


Figure 3.9. Dose-dependent percent inhibition against tyrosinase over time for: (A) Scytonemin monomer (ScyM); (B) Kojic acid (KA), the positive control compound; (C) ScyM and KA at 1 μM , 5 μM , and 25 μM , at which ScyM completely dissolves and does not have potential solubility problems.

The inhibition of tyrosinase by KA met our expectation in that the inhibition was more complete upon increasing concentrations (Figure 3.9B). However, it was surprisingly observed that while the percent inhibition for ScyM showed the same increasing trend at lower concentrations (1 μM , 5 μM and 25 μM), once the concentration was increased to 75 μM or above, it was unexpectedly decreased down to approximately 25% and remained there unchanged (Figure 3.9A). While this abnormal pattern was first thought to be due to human error introduced during the experiment, this hypothesis was refuted due to its repeatability.

Upon repeated assay at higher concentrations of ScyM (e.g. 75 μM , 150 μM and 200 μM), it was observed that there was precipitated material that accumulated at the bottom of the ScyM wells. And through more testing at various time points in the assay, this phenomenon of ScyM precipitation was detected to occur once the buffer was added, before

the tyrosinase and L-DOPA substrate were introduced into the system. This suggested that ScyM might reach its saturation point at a concentration less than 75 μM . ScyM's poor solubility in water/buffer was later found to agree with previous reports for this compound (Suyama, 2009). Consequently, we believe that this solubility issue explains the irregular inhibition trend described above. Undissolved ScyM could significantly impede the proper measurement by the plate reader, leading to an improper OD reading and hence a mistaken inhibition value. As a result, we conclude that the higher-concentration results for ScyM between 75 – 200 μM in Figure 3.9B are not illustrative of the real inhibition properties of ScyM.

Therefore, removing the high-concentration results and only considering the concentrations where ScyM was completely dissolved, as shown in Figure 3.9C, the tyrosinase inhibitory activity of ScyM was proportional to its concentration, just as for KA. Moreover, the inhibition by ScyM was always greater than KA when they were compared at the same concentration, indicating that the tyrosinase inhibitory power of ScyM could be stronger than KA. Moreover, ScyM's inhibitory effect against tyrosinase seemed to be maintained for a longer time period than KA (Figure 3.9C) in that its decrease in percent inhibition over time was less than that of KA. Consequently, these two advantages of ScyM suggest that ScyM might be a better tyrosinase inhibitor than commercially available KA. It's also important to note that the modest decrease in inhibition of tyrosinase by KA matched that of published results. This was previously interpreted as indicating that the KA-tyrosinase complex undergoes a "relatively slow reversible reaction" (Cabanés *et al.*, 1994). Accordingly, ScyM might be an "even slower" reversible inhibitor compared to KA, for its greater persistence of inhibitory effect.

Due to the solubility problems of ScyM, it was determined that all tyrosinase inhibitory assays with ScyM should subsequently be carried out in the range of 0 – 10 μM .

At these concentrations, ScyM is absolutely dissolved with no precipitate and shows strong and reproducible inhibitory activity. Therefore, to generate accurate IC₅₀ values for ScyM (and KA), HPLC purified ScyM material was used at concentrations from 0 – 10 μM. As a result, ScyM was calculated to have a lower IC₅₀ value than KA (4.9 μM vs 11.3 μM, respectively; see Table 3.2 and Figure 3.10), which supported our previous finding that ScyM has a stronger inhibitory effect against mushroom tyrosinase than the KA control. This IC₅₀ value for KA at 11.3 μM was within previously reported range from 10-300 μM and hence increased the reliability of our findings (Neeley *et al.*, 2009).

Table 3.2. Kinetic and inhibition constants of Tyrosinase by KA and ScyM.

	Substrate	K _m (mM)	V _{max} (OD·min ⁻¹)	IC ₅₀ (μM)	Inhibition mode
KA	L-Dopa	0.51 ± 0.10	13.53 ± 1.48	11.3 ± 0.8	Mixed
ScyM	L-Dopa	0.24 ± 0.05	5.98 ± 0.52	4.9 ± 0.3	Mixed

Furthermore, the IC₅₀ value of ScyM was also compared to other tyrosinase inhibitors reported in previous research by others (See Table 3.3). To put into perspective the mixed-type inhibitory potential (determined by kinetic study below) of ScyM as well as its marine origin, six other mixed-mode tyrosinase inhibitors (Table 3.3, compound 9-14) and six other marine-derived tyrosinase inhibitors (Table 3.3, compound 3-8), were chosen for comparison. Among the mixed-mode inhibitors, ScyM possesses the strongest tyrosinase inhibitory activity due to its low IC₅₀. On the other hand, in comparing to other tyrosinase inhibitors of marine origin such as the extracts of marine fungi (Li *et al.*, 2005; Wu *et al.*, 2013), ScyM compared favorably in terms of relative inhibitor potency. Furthermore, the inhibitory power of ScyM was much stronger than oscillapeptin G (IC₅₀ ≈ 100 μM), which is the only other reported tyrosinase inhibitor of a cyanobacterial origin (Sano and Kaya, 1996).

Table 3.3. Mushroom tyrosinase inhibitory activity of selected compounds from previous publications, in comparison with the positive control used in this experiment KA (1) and the compound of interest ScyM (2). References for selected compounds are listed in the bibliography at the end of chapter.

* Standard deviation not specified in the source paper.

** Inhibition mode not specified in the source paper.

	Compound	IC₅₀ (μM)	Mechanism	Reference
1	Kojic Acid (KA)	11.31 ± 0.81	Mixed	N/A
2	Scytonemin Monomer (ScyM)	4.90 ± 0.33	Mixed	N/A
3	2,3,6-tribromo-4,5-dihydroxybenzyl methyl alcohol (extract of <i>S. latiuscula</i> , a marine red algae)	270.53 ± 2.04	Competitive	Paudel <i>et al.</i> , 2019
4	bis-(2,3,6-tribromo-4,5-dihydroxybenzyl methyl ether) (extract of <i>S. latiuscula</i> , a marine red algae)	110.91 ± 4.95	Competitive	Paudel <i>et al.</i> , 2019
5	6-n-pentyl-α-pyrone (extract of marine-derived fungus <i>Myrothecium</i> sp.)	0.8*	—**	Li <i>et al.</i> , 2005
6	myrothenones A (extract of marine-derived fungus <i>Myrothecium</i> sp.)	6.6*	—**	Li <i>et al.</i> , 2005
7	1β,5α,6α,14-tetraacetoxy-9α-benzoyloxy-7β H-eudesman-2β,11-diol (extract of marine-derived fungus <i>Pestalotiopsis</i> sp. Z233)	14.8*	—**	Wu <i>et al.</i> , 2013
8	4α,5α-diacetoxy-9α-benzoyloxy-7βH-eudesman-1β,2β,11, 14-tetraol (extract of marine-derived fungus <i>Pestalotiopsis</i> sp. Z233)	22.3*	—**	Wu <i>et al.</i> , 2013
9	(<i>E</i>)-2-acetyl-5-methoxyphenyl-3-(4-methoxyphenyl)acrylate	8.3*	Mixed	Sheng <i>et al.</i> , 2018
10	(<i>E</i>)-2-isopropyl-5-methylphenyl-3-(4-hydroxyphenyl)acrylate	10.6*	Mixed	Sheng <i>et al.</i> , 2018
11	Baicalein	110*	Mixed	Guo <i>et al.</i> , 2018
12	3-phenylbenzoic acid (3-PBA)	36.3*	Mixed	Oyama <i>et al.</i> , 2016
13	Terephthalic acid	26,600 ± 2,040	Mixed	Yin <i>et al.</i> , 2011
14	Brazilein	21,210 ± 825	Mixed	Hridya <i>et al.</i> , 2015

It was also interestingly that the inhibition by purified ScyM at 10 μM was about the same as the result obtained from previous experiments using crude ScyM at 25 μM , both being approximately 60% (See Figure 3.9C and 3.10). As expected, these results indicate that pure ScyM provides stronger tyrosinase inhibitory activity than crude samples.

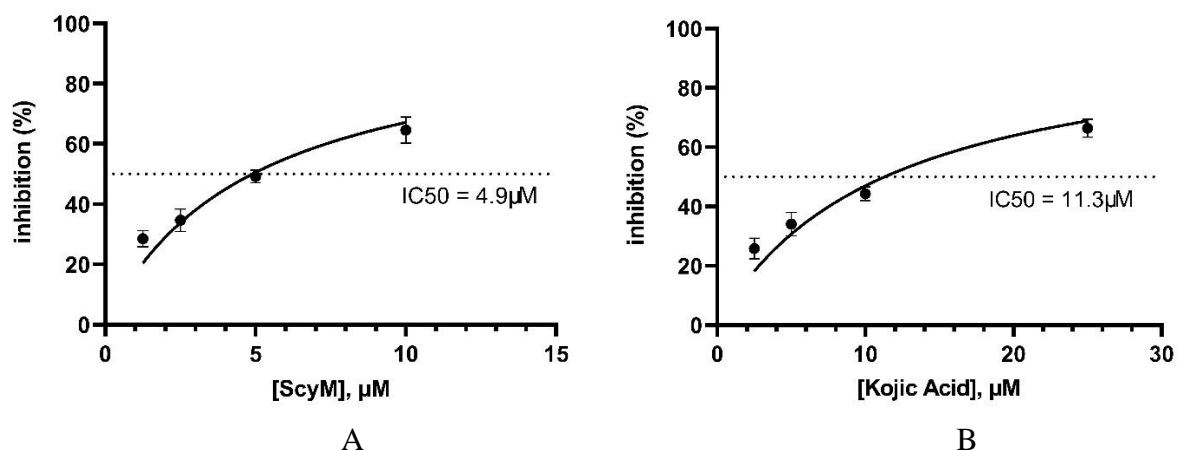


Figure 3.10. Predicted curves of tyrosinase inhibitory effect versus inhibitor concentration. (A) Scytonemin monomer (ScyM); (B) Kojic acid (KA). The dotted lines represent the IC_{50} values, which were 4.9 μM for ScyM and 11.3 μM for KA respectively.

Additionally, another set of assays was used to evaluate for synergistic effects between ScyM and KA. The combination of drugs and their potential synergism has been extensively studied in pharmacology. However, in the scope of tyrosinase inhibitor studies, most research has focused only on the inhibitory properties of single compounds rather than mixtures. Therefore, there is a very limited amount of literature on the synergistic effect of tyrosinase inhibitors (Q. Yu *et al.*, 2019). For the present study, the widely used isobologram method was selected for this analysis, and an example of isobologram analysis as well as its concept is shown in Figure 3.11.

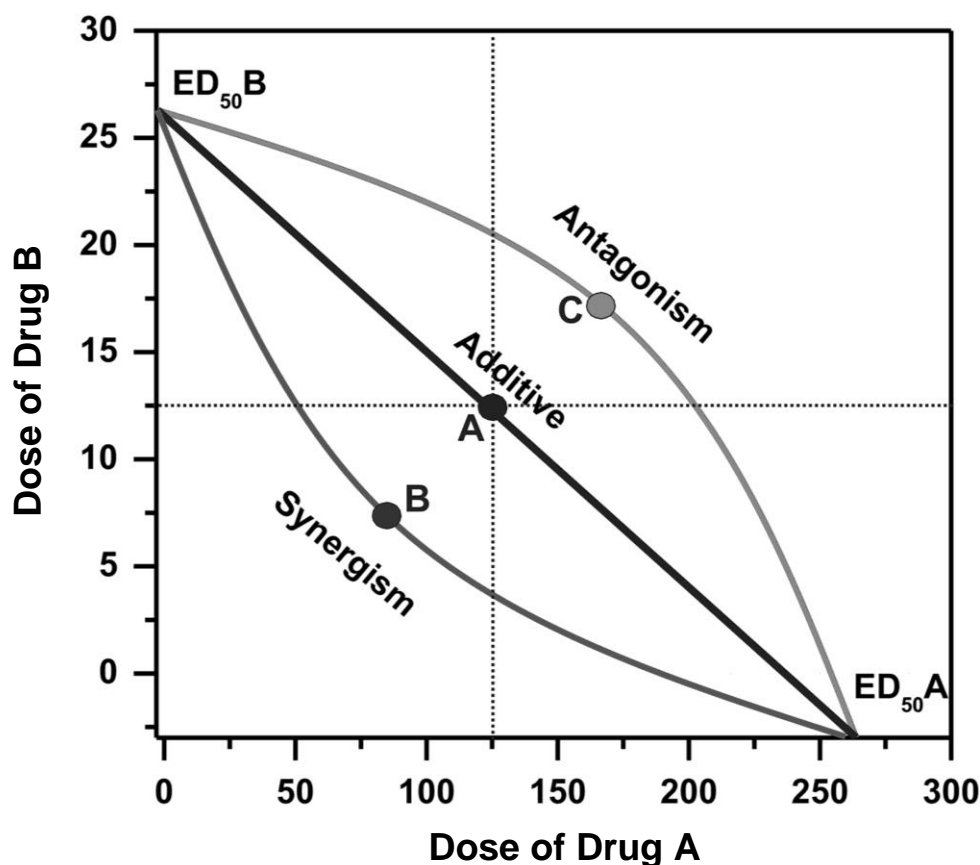


Figure 3.11. Illustration of a typical isobologram-based drug interaction analysis. The x- and y-axis represent the doses of drugs A and B, respectively. The solid black line connects doses that produce the same effect of examined response (commonly ED₅₀). If the effects of drug A and drug B are independent of each other, the ED₅₀ of mixture of A and B should theoretically fall on the straight additive line (point A). If the ED₅₀ of mixture falls below the additive line instead (point B), meaning the same effect (50% efficacy) is achieved at lower doses of the two drugs, it indicates that there is an improved effect when the two drugs are combined, which is called synergism. Vice versa, if the ED₅₀ of mixture falls above the additive line (point C), there is a reduced effect for the drug combination and the drugs hence exhibit antagonism. The dashed lines are shown to enhance the recognition of symmetry for additive isobole responses. Figure recreated from Chuang and Reddy, 2020.

Based on data from my biochemical assays, I generated the isobologram for ScyM and KA with respect to tyrosinase inhibition (Figure 3.12). The IC₅₀ values of ScyM and KA were again determined, with IC₅₀ of ScyM = 4.7 μM and IC₅₀ of KA = 10.8 μM, both being close to previous measurements (4.9 μM and 11.3 μM respectively). Next, different concentrations of ScyM and KA with a 1: 2.5 ratio were mixed and tested, and the IC₅₀ of the

mixture was determined as 2.05 μM ScyM + 5.12 μM KA. With these IC_{50} values, the isobologram for ScyM and KA was drawn, as shown in Figure 3.12A. The calculated IC_{50} of the mixture is located below the additive line, suggesting that there is synergistic inhibition of tyrosinase between ScyM and KA. The combination of the two is not independently additive in the anti-tyrosinase activity.

Alternatively, due to restricted capability of the traditional isobologram analysis in evaluating the intensity of drug interactions, we also used a complementary method to further analyze the potential for synergism between ScyM and KA. As research further improved over the isobologram method, an interaction index (γ), has been used to help better understand and mathematically describe the strength of the interacting effect of drugs (Huang *et al.*, 2019). Based on the derived equation, $\gamma = \sum_{i=2}^n \frac{d_i}{D_i}$, where D_i represents the dose of individual drug to achieve 50% efficacy when acting alone, and d_i represents the dose of each drug in the compound mixture when the combined drug achieves 50% efficacy. Accordingly, when the interactions between drugs are synergistic, additive, and antagonistic, the corresponding values of γ are < 1 , $= 1$, and > 1 respectively. The smaller the index value is, the stronger the synergistic effect would be. In our case here, the 50% efficacy is equivalent to 50% of tyrosinase inhibition or the IC_{50} values. As a result, the interaction index for ScyM and KA was calculated to be approximately 0.91, a value that is smaller than 1 and hence confirms the traditional method that a synergistic effect is observed between ScyM and KA. But because this value is close to 1.0, it also indicates that there is only a very slight synergism, which is consistent with the limited concavity of the isobologram in Figure 3.12A.

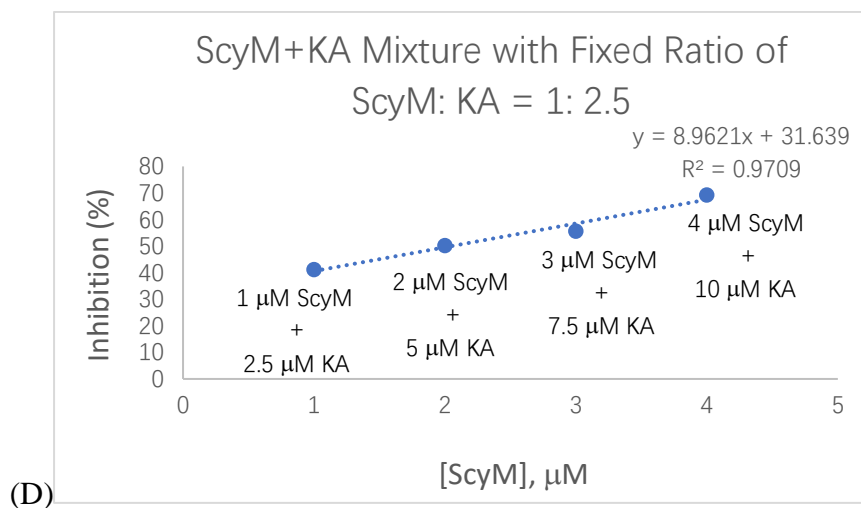
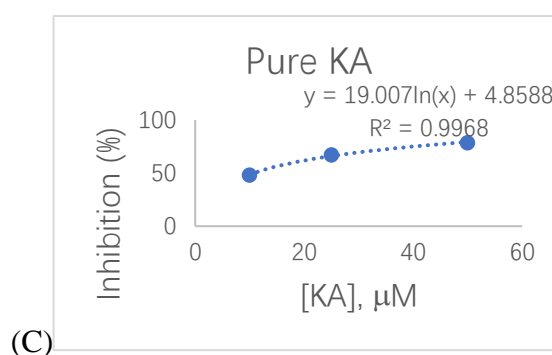
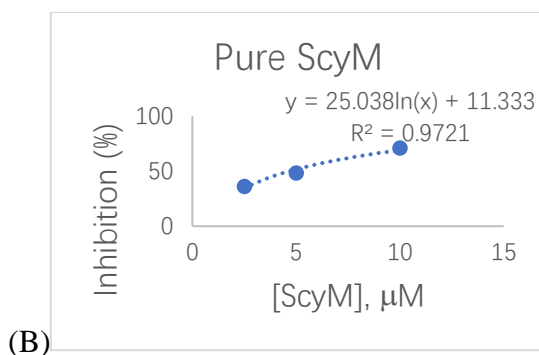
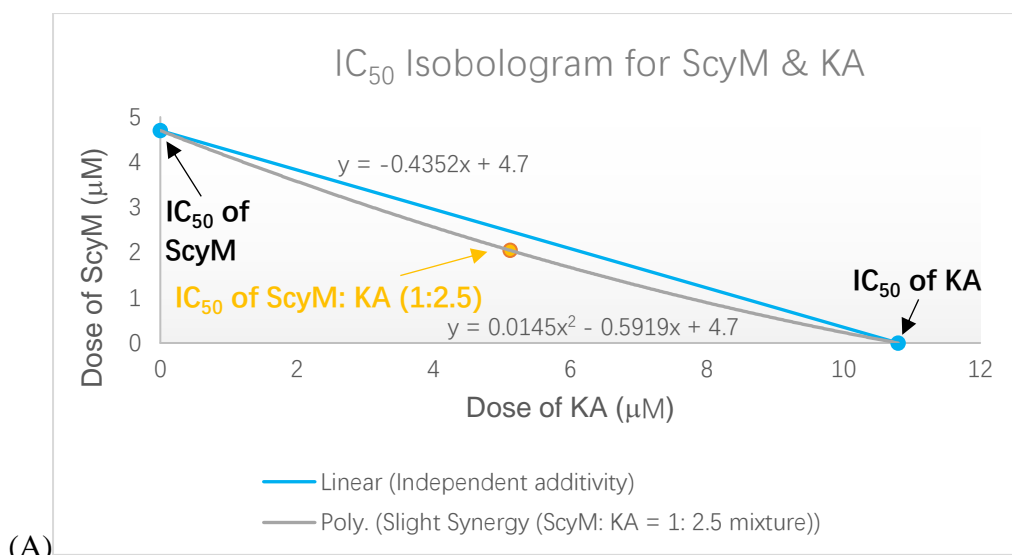


Figure 3.12. Isobologram analysis of interactions of ScyM and KA in tyrosinase inhibition. (A) IC₅₀ Isobologram for ScyM & KA. The theoretical additive line connecting the IC₅₀ values of ScyM and KA is shown in blue. And the concave grey line passing through the estimated IC₅₀ value of mixture, indicates a potential synergistic effect between the two compounds. Sub-panels (B), (C) and (D) are predicted curves to help estimate the IC₅₀ values of ScyM alone, KA alone, and mixture of ScyM and KA, respectively, to help the generation of isobologram in (A).

Kinetic analysis of mushroom tyrosinase and ScyM

A kinetic study was performed to better understand the tyrosinase inhibitory properties of ScyM. For this kinetic mode analysis, varying concentrations of substrate and inhibitor were used in the assays in order to generate Lineweaver–Burk plots. The substrate and inhibitor concentrations used in these experiments were similar to those used in previous research (Kim *et al.*, 2020). The Lineweaver–Burk plot (Figure 3.13A & 3.13B), also known as double reciprocal plot, is commonly used to determine the mechanism of how an inhibitor is inhibiting an enzyme. As its name suggests, the X-axis of the plot shows the reciprocal of substrate concentration ($[S]$), while the Y-axis shows the reciprocal of enzyme velocity ($[V]$). Meanwhile, two inhibition parameters the Michaelis–Menten constant (K_m) and maximal velocity (V_{max}) are also visualized in the plot; the x-intercept represents $-1/K_m$ and the y-intercept represents $1/V_{max}$ (Fjellstedt and Schlesselman, 1977). The apparent K_m and V_{max} values were calculated as an average of triplicates and are provided with standard deviations (see Table 3.2). The IC_{50} values representing inhibitor concentrations at which the enzyme activity is reduced by 50% are also included.

According to the Lineweaver-Burk plot (Figure 3.13A), with increasing concentrations of KA, the x-intercept moved rightward while y-intercept moved upward in the graph, demonstrating an increased K_m but decreased V_{max} ; this is an indication of a mixed mode of inhibition, as suggested in a recent kinetic study elucidating the complex pattern of tyrosinase inhibition (Deri *et al.*, 2016). Moreover, the plot itself was also consistent with a mixed inhibition mode, as both K_m and V_{max} are affected at a non-proportional rate for this type of inhibition (Miesfeld, 2017). A similar pattern was also found for ScyM (Figure 3.13B) with a V_{max} smaller than KA (Table 3.2). Consequently, ScyM also inhibits mushroom tyrosinase in a mixture of competitive and uncompetitive modes, implying that it binds to both free enzyme and the enzyme-substrate complex (Zolghadri *et al.*, 2019). The inhibition

potency of ScyM was again shown to be stronger than that of KA, as indicated by its reduced enzyme velocity (V_{\max}). Interestingly, a mixed-mode of inhibition has been frequently observed in kinetic studies of mushroom tyrosinase inhibitors (Zolghadri *et al.*, 2019). Many other compounds, such as terephthalic acid, brazilein and cinnamic acid ester derivatives, were also reported as mixed-mode mushroom tyrosinase inhibitors (Table 3.3). And these other studies also used the Lineweaver–Burk plot analysis to make this conclusion on the mode of inhibition (Yin *et al.*, 2011; Hridya *et al.*, 2015; Sheng *et al.*, 2018).

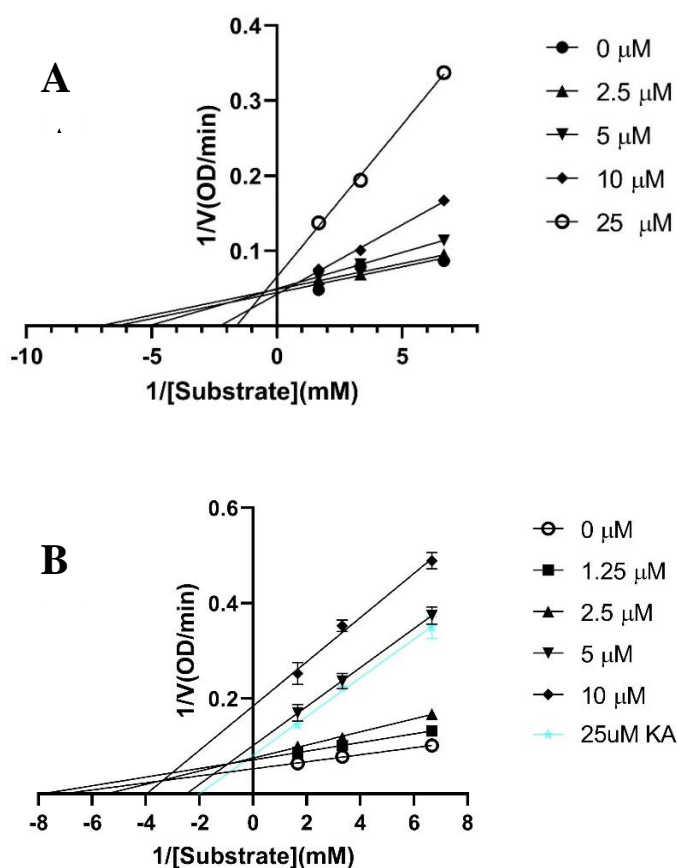


Figure 3.13. Lineweaver-Burk plots for inhibition against Mushroom Tyrosinase of A) KA, and B) ScyM. The blue line in panel B represents KA at 25 μM , which was used as the positive control in the assay.

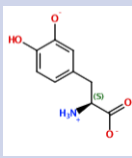
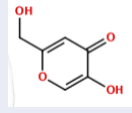
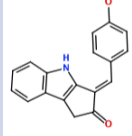
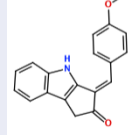
Modeling the interaction of inhibitors and substrates of mushroom tyrosinase via molecular docking

Molecular docking simulations can be used to predict the favored orientation of ligands towards target protein(s) to construct a stable complex (Hassan et al., 2018). For this reason, in-silico docking experiments are commonly used in enzyme studies as a complementary method to help understand the results of enzyme kinetic studies (Zolghadri et al., 2019). Using Molecular Operating Environment (MOE) software, different ligands including the compound of interest in this study ScyM, its methoxylated analog ScyM-OMe, the positive control KA and the natural substrate of tyrosinase L-DOPA, were separately introduced into the binding pocket of mushroom tyrosinase (PDB code: 2Y9X). This binding pocket is close to the binuclear copper binding site that is coordinated by six conserved histidine residues, as described in Chapter 1 of this thesis. The outcomes from these docking experiments are shown in Table 3.4, including all ligand interactions that were present in the top five lowest energy results.

After validation of docking accuracy using tropolone as described in the Methods section, I initiated these experiments with the natural substrate L-DOPA. The structure of L-DOPA was extracted directly from the Protein Data Bank (PDB: 4P6S). According to the best predicted conformation of the L-DOPA substrate inside the binding pocket (See Figure 3.14), the deprotonated phenol oxygen forms a metal contact with one of the copper ions. This agrees with reported catalytic functioning of tyrosinase, as the copper ions bind to the oxygen atom of the substrate and catalyze the redox reaction (Solano, 2018). Other important ligand interactions were also found: the carbonyl oxygen was found to form a hydrogen bond with Val283 and (or) Ser282 in the top 2 results, and Pi-Pi stacking and CH-Pi interactions were found for L-DOPA's aromatic ring with His263 and Val 283, respectively. Additionally, some other interactions, such as H-bond formation between the positively

charged nitrogen of L-DOPA with Met280 or Asn260, were indicated only for the binding orientations that were of somewhat lower binding energy (the lower three out of five).

Table 3.4. Results from docking assays of various inhibitors and substrates with mushroom tyrosinase, including binding energies and common ligand interactions with the binding pocket residues. Note that Pi interactions include Pi-Pi interaction, cation-Pi interaction and CH-Pi interaction.

	Structure	Best Binding Energy (Kcal/mol)	2 nd Best Binding Energy (Kcal/mol)	H-bond Interaction	Hydrophobic Interaction	Metal /ion Contact
L-DOPA		-7.20	-6.80	Val283 Ser282 Met280 Asn260 His85	His263 Val283	Cu401 Glu256
Kojic Acid		-5.51	-5.42	Met280	His263 Val283	Cu401
Deprotonated ScyM		-7.16	-7.00	Val283 Ser282 Asn81	Val283 His85	Cu401
ScyM-OMe		-5.74	-5.37	---	Val283	---

For the inhibitors, KA was found to form a metal contact with the copper ion and hydrogen bond with Met280 (See Figure 3.14). Besides, the model also suggested Pi interactions with His263 and Val283. These results for KA were consistent with experimental data from previous studies, especially those for the interactions with the Cu²⁺ ion and Met280 (Kim *et al.*, 2018; Koirala *et al.*, 2018), and provided confidence in the quality of our docking experiments.

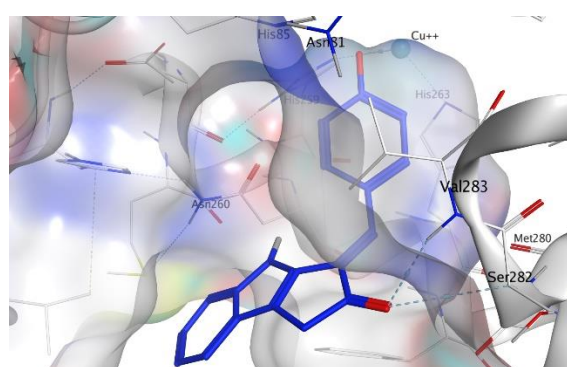
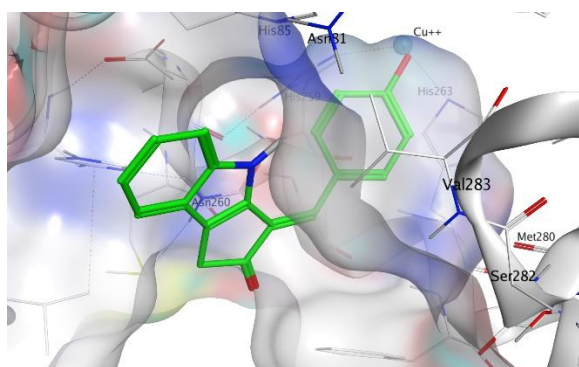
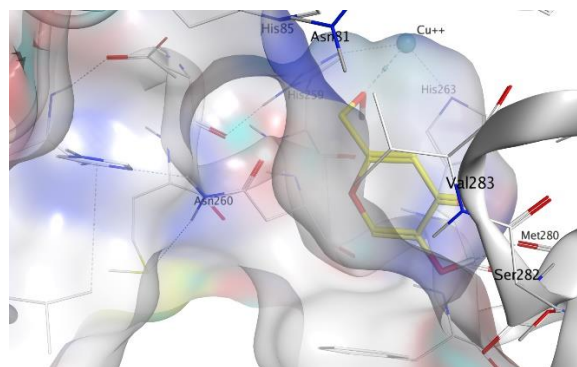
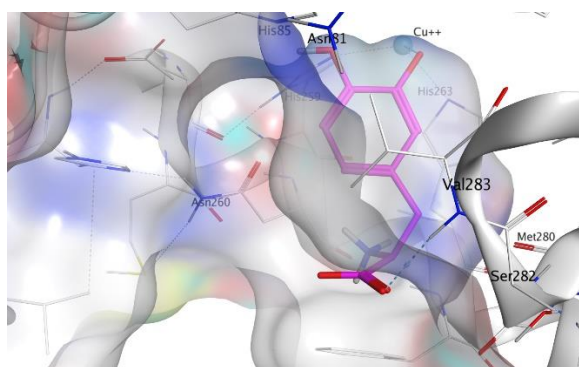
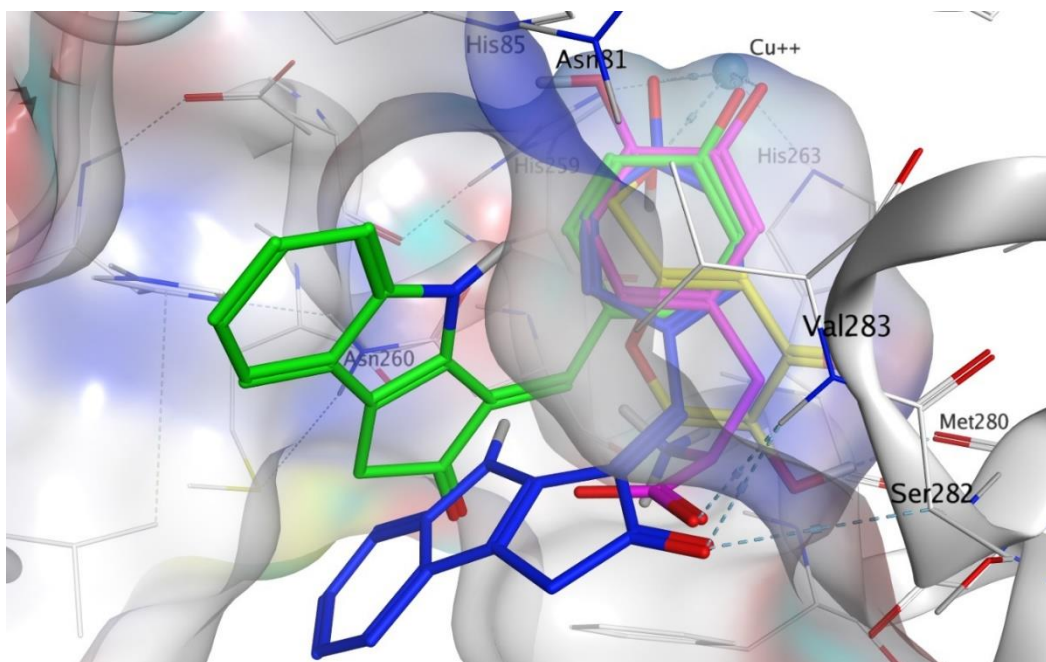


Figure 3.14. The binding conformation of L-DOPA (magenta), kojic acid (yellow), ScyM with best binding score (green) and ScyM with second-best binding score (blue). Sub-panels were provided for each individual compound to better show their interaction with nearby residues. The cyan sphere represented the copper ion in contact with ligands in pocket. Blue colored dashed lines represented the hydrogen bond formed between ligand and corresponding tyrosinase residues. Dockings of various ligands were performed separately but put together in the same plot in the composite figure for visualization of spatial overlaps.

Next, the binding conformation ScyM in mushroom tyrosinase was modeled, and the binding site was found to be close to that of the natural substrate L-DOPA. ScyM was also predicted to form a metal contact with the copper at the catalytical site (See Figure 3.14, green and blue), and the phenol moiety of ScyM was found to extensively overlap that of the catechol of L-DOPA (Figure 3.14, green, blue, and magenta). These interactions could contribute to the competitive side of the mixed-type inhibition of ScyM, as ScyM would strongly compete with the L-DOPA substrate for binding site and consequently hamper the catalytic reaction. Further, this might explain why ScyM showed stronger inhibition compared to KA as this latter compound binds further away from the L-DOPA binding site (See Figure 3.14, yellow and magenta). Another possibility is that, compared to ScyM, the lower binding energy of KA might constrain its ability to stabilize within the binding pocket and thus less efficiently inhibit substrate binding and catalysis. This analysis developed here is in agreement with the intermediate binding site proposed in previous work where KA was found able to bind at the entrance to the active site of tyrosinase (Deri et al., 2016).

Several other ligand interactions were observed among the top results from docking of ScyM to mushroom tyrosinase, including an H-bond between ScyM and Val283 & Ser282, and CH-Pi interactions with Val283. There was also a predicted hydrogen bond formed with Asn81 in poses that were of lower binding energy. Overall, a majority of these interactions between ScyM and tyrosinase were found to be similar to those found with the native substrate L-DOPA, which further supported the competitive inhibition aspect of ScyM's mixed-type inhibition. In addition, some of these interactions, such as the H-bonds with Ser282 and Asn81, as well as CH-Pi contact with Val283, matched with the docking results of other recently designed tyrosinase inhibitors (Karakaya et al., 2019). Also, the contact with Cu^{2+} was similar to that reported for many previously found tyrosinase inhibitors, providing supporting evidence that copper chelation contributes to the inhibition (Yin et al., 2011;

Şöhretoğlu et al., 2018). This similarity in findings compared with preceding work increases confidence in the validity of our findings, and also enhances the possibility that part of ScyM's inhibition of tyrosinase is mediated through metal chelation.

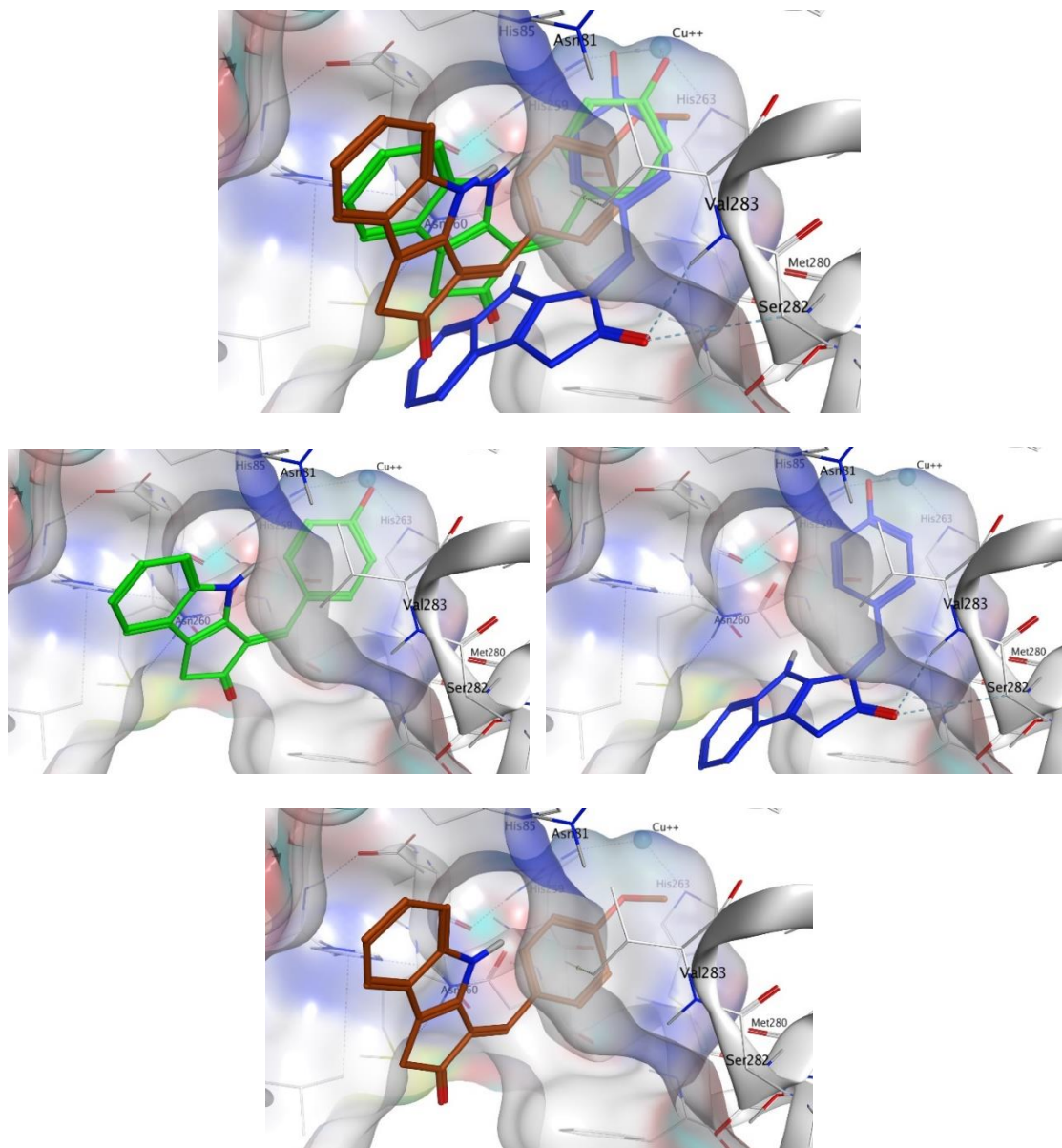


Figure 3.15. The binding conformation of ScyM with best binding score (green), ScyM with second-best binding score (blue) and ScyM-OME (brown). Sub-panels were provided for each individual compound to better show their interaction with nearby residues. The cyan sphere represents the copper ion in contact with ligands in binding pocket. Blue colored dashed lines represent hydrogen bonds between ligand and corresponding tyrosinase residues. Dockings of various ligands were performed separately but put together in the same plot in the composite figure for visualization of spatial overlaps. The methoxylated monomer ScyM-OME was no longer closely associated with the catalytic copper-binding site.

The methoxy analog ScyM-OMe was also subjected to docking experiments using MOE. As shown in Figure 3.15, replacement of the phenol hydroxy group of ScyM by the more stable methoxy group eliminated association with the copper ion, and the phenyl ring was thus located further away from the catalytic site compared to pose 1 and pose 2 of ScyM. No interaction for ScyM-OMe was observed with tyrosinase except Pi-Sigma contact with the Val283 residue. Moreover, the binding energy decreased dramatically for ScyM-OMe, from above -7 Kcal/mol to only -5.74 Kcal/mol (see Table 3.4). These findings corresponded with our experimental data from tyrosinase inhibitory assays subsequently performed with ScyM-OMe. At a concentration of 35 μ M, there was only about 1% inhibition of tyrosinase activity, indicating very little inhibitory activity remaining after this structural modification. Therefore, from a combination of *in silico* docking and *in vitro* assays, it appears that the phenol moiety is largely responsible and necessary for the mixed-type tyrosinase inhibitory activity of ScyM. This conclusion agrees quite well with the literature which suggested an evident correlation between potent tyrosinase-inhibitory effects and compounds with hydroxyl groups (Lima et al., 2014).

Lastly, besides the competitive aspect of inhibition described above, we hypothesize that the uncompetitive aspect of ScyM's mixed-type inhibition might be because it could also serve as substrate for the mushroom tyrosinase. Tyrosinase has both monophenolase (L-tyrosine as natural substrate) and diphenolase (L-DOPA as natural substrate) activities. Considering the similarity of the phenol head of ScyM which is shared by L-tyrosine (See Figure 2.1 for structure), it seems reasonable that tyrosinase may be also capable to catalyze hydroxylation of ScyM to form a diphenol, resembling conversion from L-tyrosine to L-DOPA. To test this hypothesis, currently an incubation experiment is ongoing using ScyM and mushroom tyrosinase, with the prediction that there will be an addition of one more hydroxyl group to the phenyl ring of ScyM.

Inhibition of tyrosinase by scytonemin vs. scytonemin monomer (ScyM)

The tyrosinase inhibitory properties that we found for ScyM led us to wonder if similar properties would be present for its dimeric structure, the cyanobacterial sunscreen pigment scytonemin. Therefore, a dose-dependent assay was also performed for scytonemin. Curiously, the results revealed that at all concentrations tested, from 1 μM up to 200 μM , there was almost no inhibition by scytonemin (Figure 3.16). These results were considered valid as the positive and negative controls functioned properly, showing percent inhibitions similar to previous assays (See Figure 3.9B & 3.16). Therefore, scytonemin is not a tyrosinase inhibitor, perhaps because the dimeric scytonemin molecule is too large for the catalytic site of tyrosinase and thus can no longer participate in ligand interactions with surrounding residues as does ScyM. In order to further explore this hypothesis, I performed a docking experiment with scytonemin using the methods described earlier in which the scytonemin molecule was inserted into the binding pocket of mushroom tyrosinase and evaluated for best poses.

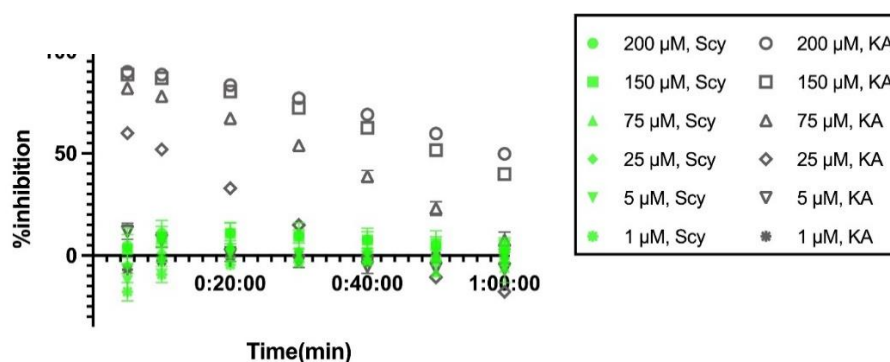


Figure 3.16. Dose dependent percent inhibition of mushroom tyrosinase by scytonemin and kojic acid over time. Shown in green are the results of scytonemin and in grey are the results of the positive control kojic acid (KA).

Unexpectedly, the docking result showed that deprotonated scytonemin could achieve a similar positioning inside the enzyme pocket just as ScyM, and could make a similar metal contact with the Cu^{2+} just like L-DOPA, ScyM and the other substrates discussed above. The

top two poses of scytonemin gave binding energy of -8.23 Kcal/mol and -8.16 Kcal/mol respectively, indicating an even greater binding of scytonemin to tyrosinase than ScyM. This result could be interpreted as that scytonemin might also retain robust binding to mushroom tyrosinase, if its phenol head could be secured inside the binding pocket. However, it is possible that this better binding score might be partially attributed to the portion of its larger structure that is exposed outside of the pocket, and might hence be artificially higher and not reflective of its real binding affinity to the ligand binding site. The interaction of scytonemin with Phe264 and Val248 residues of tyrosinase, both of which are quite distant from the catalytic copper-binding pocket and the conserved histidine residues, supports such idea (See Figure 3.17).

In addition to the possibility that in-silico poses are over idealized and scytonemin is too large to have its phenol moiety properly bind in the substrate pocket *in vitro*, in its best five poses it was found to not form an H-bond with Val283 and Ser282, unlike ScyM (Table 3.4). The lack of a strong non-covalent interaction and only Pi interactions mediating the positioning of scytonemin alone, may result in a lack of stabilization of the molecule inside the binding site. This would further result in a lack of contact by scytonemin with the copper ion which is crucial for inhibitory activity.

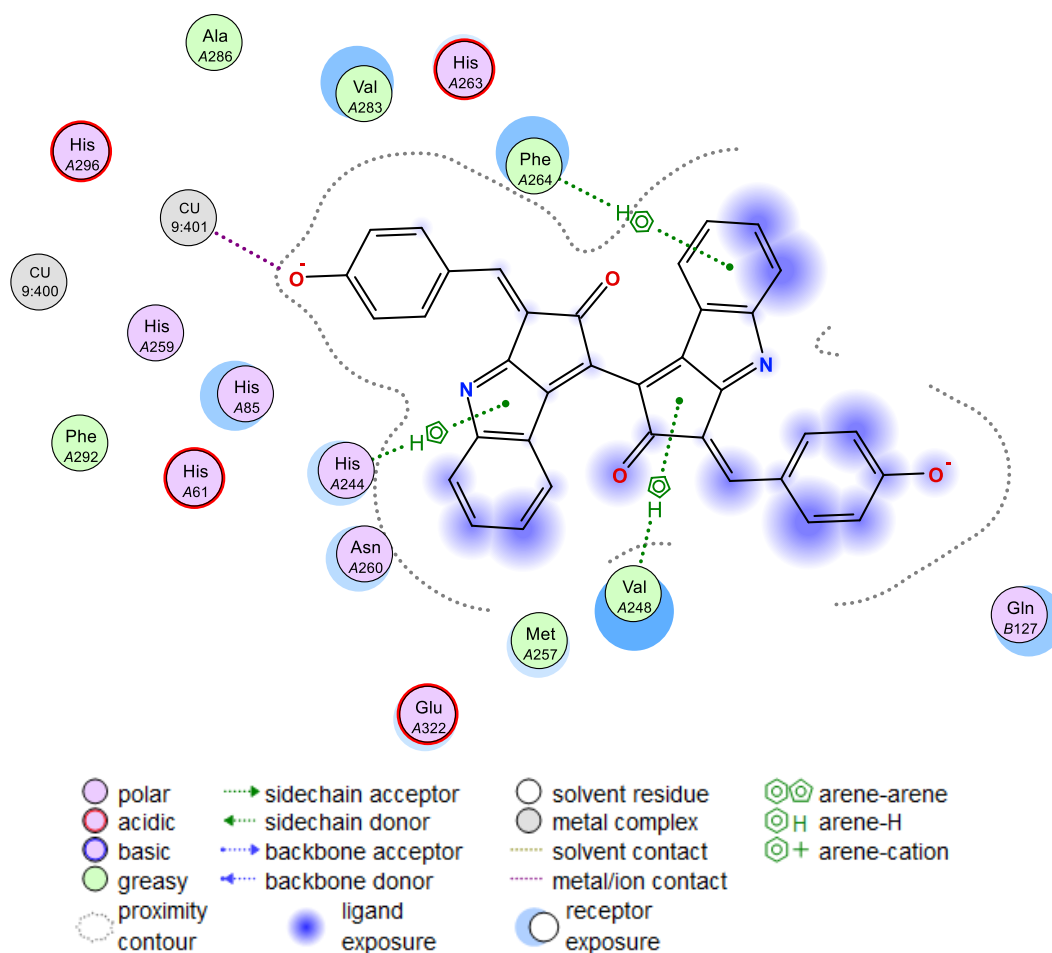


Figure 3.17. Predicted ligand interaction of scytonemin and mushroom tyrosinase based on spatial orientation with highest binding score from docking experiment.

Besides the difference in anti-tyrosinase activity, results from other assays have also shown variations in the bioactivity of scytonemin versus ScyM. Matsui *et al.* first proposed in 2012 that scytonemin is a slow-acting radical scavenger that reacts with ABTS, but not DPPH radical which was known for selectivity for scavengers with strong scavenging activity. Results from another screening project carried in Gerwick Lab using the DPPH assay and samples from our compound library by Yi Zhang in 2019 (unpublished), confirmed this idea as scytonemin was quite inactive in that assay. But interestingly, ScyM was identified as having DPPH scavenging rate of ~35% (See Figure 3.18), which was one of the most potent compounds discovered in that assay. It was also over half of the score for Trolox (~53%), a commonly used positive control in DPPH assays. Consequently, ScyM was also

considered to have antioxidant activity while scytonemin does not. Additionally, our cytotoxicity assay revealed ScyM to be non-cytotoxic, as no significant effect was observed for H460 human lung cancer cells at concentration as high as 254 μ M. Scytonemin was also reported to be non-cytotoxic in several research reports (Malla and Sommer, 2014; Kang *et al.*, 2020).

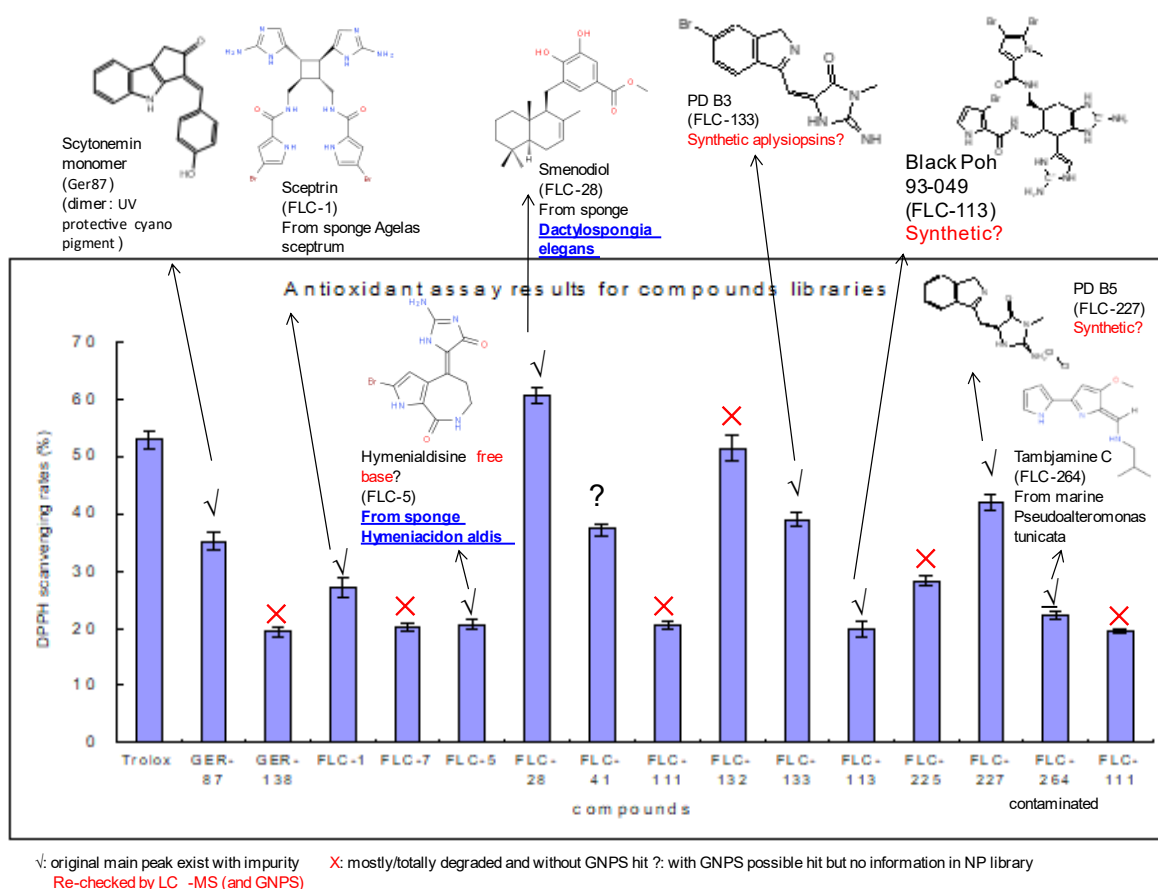


Figure 3.18. Screening result from DPPH assay showing scytonemin monomer (ScyM) has modest antioxidant activity. Trolox, the positive control, is the furthest bar to the left.

IV. Conclusion

After re-synthesis and further purification, ScyM was successfully validated for its structure using MS and NMR data. Upon more testing using the replenished material, ScyM was discovered to possess a mixed-type inhibition against mushroom tyrosinase, with an $IC_{50} = 4.90 \mu\text{M}$. Combined with its better duration of inhibition, properly dissolved ScyM not only outcompeted many other compounds with anti-tyrosinase activity, but also was a better tyrosinase inhibitor than kojic acid (KA), which is a commercially available standard inhibitor and has an IC_{50} value of $11.31 \mu\text{M}$ in our assay. Meanwhile, slight synergism of the ScyM and KA was observed upon *in vitro* testing. Additionally, based on molecular docking, ScyM was found to locate inside the binding pocket with good binding affinity, and the location was in close proximity with the L-DOPA substrate binding site. Its ligand interaction with Cu^{2+} , along with several other interactions with nearby amino acid residues in the binding pocket, secures its position. In this regard, it appears that ScyM can function as a copper chelator, just like many other tyrosinase inhibitors determined in the past. These reasons together might explain the fundamental inhibitory mechanism of ScyM against tyrosinase. From the docking experiments, it also appears that the phenol moiety of ScyM, which resembles the functional component of the natural substrate L-DOPA, was indeed the part responsible for the inhibiting effect. Once the hydroxy group was replaced with a methoxy group, ScyM was no longer able to bind tightly inside the pocket and lost its inhibitory activity *in vitro*. On the other hand, the dimeric cyanobacterial sunscreen pigment scytonemin was inactive as an inhibitor, although the docking studies suggested that it should theoretically have a robust binding affinity to the pocket. The larger sized structure of scytonemin as well as the lack of strong non-covalent interactions with the tyrosinase pocket residues is proposed to explain scytonemin's lack of inhibitory property.

Reference

- Balskus EP, Walsh CT. (2008) Investigating the initial steps in the biosynthesis of cyanobacterial sunscreen scytonemin. *J Am Chem Soc.* 130(46):15260–15261.
- Balskus EP, Walsh CT. (2009) An enzymatic cyclopentyl[b]indole formation involved in scytonemin biosynthesis. *J Am Chem Soc.* 131(41):14648–14649.
- Buitrago E, Hardré R, Haudecoeur R, Jamet H, Belle C, Boumendjel A, Bubacco L, Réglier M. (2016) Are human tyrosinase and related proteins suitable targets for melanoma therapy? *Curr Top Med Chem.* 16(27):3033–3047.
- Cabanes J, Chazarra S, Garcia-Carmona F. (1994) Kojic acid, a cosmetic skin whitening agent, is a slow-binding inhibitor of catecholase activity of tyrosinase. *J Pharm Pharmacol.* 46(12):982–985.
- Chuang S-H, Reddy DS. (2020) Isobolographic analysis of antiseizure activity of the GABA type A receptor-modulating synthetic neurosteroids brexanolone and ganaxolone with tiagabine and midazolam. *J Pharmacol Exp Ther.* 372(3):285–298.
- Deri B, Kanteev M, Goldfeder M, Lecina D, Guallar V, Adir N, Fishman A. (2016) The unravelling of the complex pattern of tyrosinase inhibition. *Sci Rep.* 6:34993.
- Ekebergh A, Karlsson I, Mete R, Pan Y, Börje A, Mårtensson J. (2011) Oxidative coupling as a biomimetic approach to the synthesis of scytonemin. *Org Lett.* 13(16):4458–4461.
- Ferreira D, Garcia-Pichel F. (2016) Mutational studies of putative biosynthetic genes for the cyanobacterial sunscreen scytonemin in *Nostoc punctiforme* ATCC 29133. *Front Microbiol.* 7:735.
- Fields, P.A. (2011) Temperature | Proteins and Temperature, *Encycl. Fish Physiol.* 3: 1703–17
- Fjellstedt TA, Schlesselman JJ. (1977) A simple statistical method for use in kinetic analysis based on Lineweaver-Burk plots. *Anal Biochem.* 80(1):224–238.
- Gao Q, Garcia-Pichel F. (2011) Microbial ultraviolet sunscreens. *Nat Rev Microbiol.* 9(11):791–802.
- Garcia-Pichel F, Castenholz RW. (1991) Characterization and biological implications of scytonemin, a cyanobacterial sheath pigment. *J Phycol.* 27(3):395–409.
- Guo N, Wang C, Shang C, You X, Zhang L, Liu W. (2018) Integrated study of the mechanism of tyrosinase inhibition by baicalein using kinetic, multispectroscopic and computational simulation analyses. *Int J Biol Macromol.* 118:57–68.
- Hassan M, Ashraf Z, Abbas Q, Raza H, Seo S-Y. (2018) Exploration of novel human tyrosinase inhibitors by molecular modeling, docking and simulation studies. *Interdiscip Sci.* 10(1):68–80.

- Helms GL, Moore RE, Niemczura WP, Patterson GML, Tomer KB, Gross ML. (1988) Scytonemin A, a novel calcium antagonist from a blue-green alga. *J Org Chem.* 53(6):1298–1307.
- Hridya H, Amrita A, Sankari M, George Priya Doss C, Gopalakrishnan M, Gopalakrishnan C, Siva R. (2015) Inhibitory effect of brazilein on tyrosinase and melanin synthesis: Kinetics and in silico approach. *Int J Biol Macromol.* 81:228–234.
- Huang R-Y, Pei L, Liu Q, Chen S, Dou H, Shu G, Yuan Z-X, Lin J, Peng G, Zhang W and Fu H. (2019) Isobologram analysis: A comprehensive review of methodology and current research. *Front Pharmacol.* 10:1222.
- Ismaya WT, Rozeboom HJ, Weijn A, Mes JJ, Fusetti F, Wichers HJ, Dijkstra BW. (2011) Crystal structure of *Agaricus bisporus* mushroom tyrosinase: identity of the tetramer subunits and interaction with tropolone. *Biochemistry.* 50(24):5477–5486.
- Itoh T, Koketsu M, Yokota N, Touho S, Ando M, Tsukamasa Y. (2014) Reduced scytonemin isolated from *Nostoc commune* suppresses LPS/IFN γ -induced NO production in murine macrophage RAW264 cells by inducing hemeoxygenase-1 expression via the Nrf2/ARE pathway. *Food Chem Toxicol.* 69:330–338.
- Janssen J, Soule T. (2016) Gene expression of a two-component regulatory system associated with sunscreen biosynthesis in the cyanobacterium *Nostoc punctiforme* ATCC 29133. *FEMS Microbiol Lett.* 363(2): fmv235.
- Jones CS, Esquenazi E, Dorrestein PC, Gerwick WH. (2011) Probing the in vivo biosynthesis of scytonemin, a cyanobacterial ultraviolet radiation sunscreen, through small scale stable isotope incubation studies and MALDI-TOF mass spectrometry. *Bioorg Med Chem.* 19(22):6620–6627.
- Kang MR, Jo SA, Lee H, Yoon YD, Kwon J-H, Yang J-W, Choi BJ, Park KH, Lee MY, Lee CW. (2020) Inhibition of skin inflammation by scytonemin, an ultraviolet sunscreen pigment. *Mar Drugs.* 18(6):300.
- Karakaya G, Türe A, Ercan A, Öncül S, Aytemir MD. (2019) Synthesis, computational molecular docking analysis and effectiveness on tyrosinase inhibition of kojic acid derivatives. *Bioorg Chem.* 88(102950):102950.
- Kim CS, Noh SG, Park Y, Kang D, Chun P, Chung HY, Jung HJ, Moon HR. (2018) A potent tyrosinase inhibitor, (E)-3-(2,4-dihydroxyphenyl)-1-(thiophen-2-yl)prop-2-en-1-one, with anti-melanogenesis properties in α -MSH and IBMX-induced B16F10 melanoma cells. *Molecules.* 23(10):2725.
- Kim JH, Jang DH, Lee KW, Kim KD, Shah AB, Zhumanova K, Park KH. (2020) Tyrosinase inhibition and kinetic details of puerol A having but-2-enolide structure from *Amorpha fruticosa*. *Molecules.* 25(10):2344.
- Klicki K, Ferreira D, Hamill D, Dirks B, Mitchell N, Garcia-Pichel F. (2018) The Widely Conserved ebo Cluster Is Involved in Precursor Transport to the Periplasm during Scytonemin Synthesis in *Nostoc punctiforme*. *MBio.* 9(6). doi:10.1128/mBio.02266-18.

- Koirala P, Seong SH, Zhou Y, Shrestha S, Jung HA, Choi JS. (2018) Structure-Activity relationship of the tyrosinase inhibitors kuwanon G, mulberrofuran G, and albanol B from *Morus* species: A kinetics and molecular docking study. *Molecules*. 23(6):1413.
- Leber CA, Naman CB, Keller L, Almaliti J, Caro-Diaz EJE, Glukhov E, Joseph V, Sajeevan TP, Reyes AJ, Biggs JS, Li T, Yuan Y, He S, Yan X-J, Gerwick WH. (2020) Applying a chemogeographic strategy for natural product discovery from the marine Cyanobacterium *Moorea bouillonii*. *Mar Drugs*. 18(10). doi:10.3390/md18100515.
- Li X, Kim MK, Lee U, Kim S-K, Kang JS, Choi HD, Son BW. (2005) Myrothenones A and B, cyclopentenone derivatives with tyrosinase inhibitory activity from the marine-derived fungus *Myrothecium* sp. *ChemInform*. 36(39). doi:10.1002/chin.200539194.
- Lima CR, Silva JRA, de Tássia Carvalho Cardoso E, Silva EO, Lameira J, do Nascimento JLM, do Socorro Barros Brasil D, Alves CN. (2014) Combined kinetic studies and computational analysis on kojic acid analogous as tyrosinase inhibitors. *Molecules*. 19(7):9591–9605.
- Malla S, Sommer MOA. (2014) A sustainable route to produce the scytonemin precursor using *Escherichia coli*. *Green Chem*. 16(6):3255–3265.
- Mathews C.K., van Holde K.E., Ahern K.G. (2000) Photosynthesis. Biochemistry 3rd edition. *Addison Wesley Longman, Inc: USA*. 601.
- Matsui K, Nazifi E, Hirai Y, Wada N, Matsugo S, Sakamoto T. (2012) The cyanobacterial UV-absorbing pigment scytonemin displays radical-scavenging activity. *J Gen Appl Microbiol*. 58(2):137–144.
- Miesfeld RL, McEvoy MM. (2016) Biochemistry. New York, NY: *W.W. Norton & Company*. pp. 340–370.
- Nägeli, Carl. Gattungen einzelliger Algen: physiologisch und systematisch bearbeitet. Friedrich Schulthess, 1849.
- Neeley E, Fritch G, Fuller A, Wolfe J, Wright J, Flurkey W. (2009) Variations in IC(50) values with purity of mushroom tyrosinase. *Int J Mol Sci*. 10(9):3811–3823.
- Oyama T, Takahashi S, Yoshimori A, Yamamoto T, Sato A, Kamiya T, Abe H, Abe T, Tanuma S-I. (2016) Discovery of a new type of scaffold for the creation of novel tyrosinase inhibitors. *Bioorg Med Chem*. 24(18):4509–4515.
- Pathak J, Pandey A, Maurya PK, Rajneesh R, Sinha RP, Singh SP. (2020) Cyanobacterial secondary metabolite scytonemin: A potential photoprotective and pharmaceutical compound. *Proc Natl Acad Sci India Sect B Biol Sci*. 90(3):467–481.
- Paudel P, Wagle A, Seong SH, Park HJ, Jung HA, Choi JS. (2019) A new tyrosinase inhibitor from the red alga *Symphyclocladia latiuscula* (Harvey) Yamada (Rhodomelaceae). *Mar Drugs*. 17(5):295.

- Proteau PJ, Gerwick WH, Garcia-Pichel F, Castenholz R. (1993) The structure of scytonemin, an ultraviolet sunscreen pigment from the sheaths of cyanobacteria. *Experientia*. 49(9):825–829.
- Rodríguez JG, Urrutia A, Canoira L. (1996) Electron impact mass spectrometry of indole derivatives. *Int J Mass Spectrom Ion Process*. 152(2–3):97–110.
- Roy S. (2017) Impact of UV radiation on genome stability and human health. *Adv Exp Med Biol*. 996:207–219.
- Sano T, Kaya K. (1996) Oscillapeptin G, a tyrosinase inhibitor from toxic *Oscillatoria agardhii*. *J Nat Prod*. 59(1):90–92.
- Sheng Z, Ge S, Xu Ximing, Zhang Y, Wu P, Zhang K, Xu Xuetao, Li C, Zhao D, Tang X. (2018) Design, synthesis and evaluation of cinnamic acid ester derivatives as mushroom tyrosinase inhibitors. *Med chem comm*. 9(5):853–861.
- Şöhretoğlu D, Sari S, Barut B, Özel A. (2018) Tyrosinase inhibition by some flavonoids: Inhibitory activity, mechanism by in vitro and in silico studies. *Bioorg Chem*. 81:168–174.
- Solano F. (2018) On the metal cofactor in the tyrosinase family. *Int J Mol Sci*. 19(2):633.
- Sorrels CM, Proteau PJ, Gerwick WH. (2009) Organization, evolution, and expression analysis of the biosynthetic gene cluster for scytonemin, a cyanobacterial UV-absorbing pigment. *Appl Environ Microbiol*. 75(14):4861–4869.
- Soule T, Garcia-Pichel F, Stout V. (2009) Gene expression patterns associated with the biosynthesis of the sunscreen scytonemin in *Nostoc punctiforme* ATCC 29133 in response to UVA radiation. *J Bacteriol*. 191(14):4639–4646.
- Soule T, Palmer K, Gao Q, Potrafka RM, Stout V, Garcia-Pichel F. (2009) A comparative genomics approach to understanding the biosynthesis of the sunscreen scytonemin in cyanobacteria. *BMC Genomics*. 10:336.
- Soule T, Stout V, Swingley WD, Meeks JC, Garcia-Pichel F. (2007) Molecular genetics and genomic analysis of scytonemin biosynthesis in *Nostoc punctiforme* ATCC 29133. *J Bacteriol*. 189(12):4465–4472.
- Stevenson CS, Capper EA, Roshak AK, Marquez B, Eichman C, Jackson JR, Mattern M, Gerwick WH, Jacobs RS, Marshall LA. (2002) The identification and characterization of the marine natural product scytonemin as a novel antiproliferative pharmacophore. *J Pharmacol Exp Ther*. 303(2):858–866.
- Suyama T. (2009) Organic synthesis as an effective approach to chemical, pharmaceutical, and biosynthetic investigations of natural products. Ph.D. Dissertation. University of California, San Diego.

- Wu B, Wu X, Sun M, Li M. (2013) Two novel tyrosinase inhibitory sesquiterpenes induced by CuCl₂ from a marine-derived fungus *Pestalotiopsis* sp. Z233. *Mar Drugs*. 11(8):2713–2721.
- Yin S-J, Si Y-X, Chen Y-F, Qian G-Y, Lü Z-R, Oh S, Lee J, Lee S, Yang J-M, Lee D-Y, Park Y-D. (2011) Mixed-type inhibition of tyrosinase from *Agaricus bisporus* by terephthalic acid: computational simulations and kinetics. *Protein J*. 30(4):273–280.
- Yu H-B, Glukhov E, Li Y, Iwasaki A, Gerwick L, Dorrestein PC, Jiao B-H, Gerwick WH. (2019) Cytotoxic Microcolin Lipopeptides from the Marine Cyanobacterium *Moorea producens*. *J Nat Prod*. 82(9):2608–2619.
- Yu Q, Fan L, Duan Z. (2019) Five individual polyphenols as tyrosinase inhibitors: Inhibitory activity, synergistic effect, action mechanism, and molecular docking. *Food Chem*. 297(124910):124910.
- Zolghadri S, Bahrami A, Hassan Khan MT, Munoz-Munoz J, Garcia-Molina F, Garcia-Canovas F, Saboury AA. (2019) A comprehensive review on tyrosinase inhibitors. *J Enzyme Inhib Med Chem*. 34(1):279–309.

CHAPTER FOUR

CONCLUSION

Even though there have been advances in screening methodology and analytical chemistry instrumentation and tools, which allow NP researchers to gather important information about extract libraries from the earliest stages of the drug discovery process, the fundamental and traditional methods of assay-guided isolation of bioactive NPs still remain effective for discovering new compounds or for finding new purposes of previously known compounds (Miller, 2016). The screening campaign for potential mushroom tyrosinase inhibitors, described in Chapter 2, exemplifies the latter idea, and was conducted in response to the demand for more tyrosinase inhibitors. Specifically, our study aimed at NPs from marine algae and cyanobacteria, which were understudied as potential sources of tyrosinase inhibitors. By using classic colorimetric assays, six hits were initially identified from Gerwick Laboratory compound library. The pure compound, scytonemin monomer (ScyM), was confirmed for its tyrosinase inhibitory activity after multiple re-validating dose-dependent tests to exclude false positives, and hence selected for in-depth evaluation in chapter 3.

ScyM has been proposed to be the final precursor in the scytonemin biosynthetic pathway in previous publications (Balskus and Walsh, 2008; Balskus and Walsh, 2009). In chapter 3, I confirmed its structure through mass spectrometry and nuclear magnetic resonance spectroscopy, and then ScyM was subjected to more bioassays. The IC_{50} value of ScyM generated based on experiments, as well as a converted K_i value based on a published web-server tool (Cer *et al.*, 2009), appears to be lower compared to that of a commercially available standard tyrosinase inhibitor, Kojic Acid (KA).

Together with its observed longer duration of inhibition, ScyM was determined to have better tyrosinase inhibitory potency not only than KA, but also many other tyrosinase inhibitors reported in the literature. We also found via enzyme kinetics analysis and Lineweaver-Burk plots that, ScyM, as well as KA, retains mixed-type inhibition against mushroom tyrosinase. This mode of inhibition has also been frequently observed in kinetic studies of other inhibitors (Oyama *et al.*, 2016; Guo *et al.*, 2018). Additionally, based on *in silico* molecular docking, ScyM was found to successfully locate inside the binding pocket with good predicted binding affinity, and the binding site was in close proximity to that of tyrosinase's natural substrate, L-DOPA. The ligand interactions observed in the docking study suggested the possibility that ScyM functions as a copper chelator, similar to many other tyrosinase inhibitors defined previously (Yin *et al.*, 2011; Şöhretoğlu *et al.*, 2018). From the docking experiments, it also appears that the phenol moiety of ScyM, which resembles the functional component of the natural substrate L-DOPA, was indispensable for its inhibitory effect. If the phenol was replaced with the more stable methoxy group, ScyM was no longer capable of binding tightly inside the pocket, verifying our experimental results that showed a complete loss of inhibitory activity *in vitro* for this derivative. Additionally, the dimeric cyanobacterial sunscreen pigment scytonemin was shown to be inactive as an inhibitor against mushroom tyrosinase in the assays. The oversized structure of scytonemin, as well as the lack of strong non-covalent interactions with the binding pocket residues shown in docking experiment, are proposed to explain this lack of inhibitory property.

As for future perspectives, the relationship between ScyM and mushroom tyrosinase may suggest additional insights into the biosynthetic gene cluster (BGC) study of the cyanosunscreen pigment scytonemin. As a partial explanation for the uncompetitive aspect of ScyM's mixed-type inhibition, we propose that ScyM might also be able to serve as substrate for the mushroom tyrosinase. Because there is also predicted tyrosinase enzyme (Npr1263)

found present in the gene cluster of scytonemin-producing cyanobacteria *N. punctiforme* ATCC 29133, it is possible that this enzyme is involved in the *in vivo* mechanism of scytonemin dimerization. The results from our ongoing incubation experiments of ScyM and mushroom tyrosinase support this conjecture.

Additionally, in order to broaden the application of ScyM as human skin-whitening agent to treat freckles and age-spots of human in the future, it is important for ScyM to be tested against human tyrosinase. Despite the fact that human tyrosinase and mushroom tyrosinase have long been recognized as possessing a high similarity and homology (Ismaya *et al.*, 2011), the amino acid sequence identity between these two enzymes is only 23% (Sugimoto *et al.*, 2003). And considering previous findings that the activity of a tyrosinase inhibitor can be different depending on the different source of an enzyme (Zolghadri *et al.*, 2019), it would be interesting to study if ScyM performs equally well against human tyrosinase.

In conclusion, this project successfully identified ScyM as the second case ever of a novel tyrosinase inhibitory compound from a marine cyanobacterium. We hope it opens the possibility that future research on other cyanobacterial-derived natural products, as well as some mycosporine-like amino acids (MAAs) which are also known as “microbial sunscreens” (Oren and Gunde-Cimerman, 2007), will reveal additional anti-tyrosinase compounds with promising pharmaceutical and cosmeceutical value.

Reference

- Balskus EP, Walsh CT. (2008) Investigating the initial steps in the biosynthesis of cyanobacterial sunscreen scytonemin. *J Am Chem Soc.* 130(46):15260–15261.
- Balskus EP, Walsh CT. (2009) An enzymatic cyclopentyl[b]indole formation involved in scytonemin biosynthesis. *J Am Chem Soc.* 131(41):14648–14649.
- Cer RZ, Mudunuri U, Stephens R, Lebeda FJ. (2009) IC50-to-Ki: a web-based tool for converting IC50 to Ki values for inhibitors of enzyme activity and ligand binding. *Nucleic Acids Res.* 37(Web Server issue): W441-5.
- Guo N, Wang C, Shang C, You X, Zhang L, Liu W. (2018) Integrated study of the mechanism of tyrosinase inhibition by baicalein using kinetic, multispectroscopic and computational simulation analyses. *Int J Biol Macromol.* 118:57–68.
- Ismaya WT, Rozeboom HJ, Weijn A, Mes JJ, Fusetti F, Wichers HJ, Dijkstra BW. (2011) Crystal structure of *Agaricus bisporus* mushroom tyrosinase: identity of the tetramer subunits and interaction with tropolone. *Biochemistry.* 50(24):5477–5486.
- Miller BW. (2016) Marine Natural Products as Modulators of Human Cathepsin Proteases. Ph.D. Dissertation. University of California, San Diego.
- Oren A, Gunde-Cimerman N. 2007. Mycosporines and mycosporine-like amino acids: UV protectants or multipurpose secondary metabolites? *FEMS Microbiol Lett.* 269(1):1–10.
- Oyama T, Takahashi S, Yoshimori A, Yamamoto T, Sato A, Kamiya T, Abe H, Abe T, Tanuma S-I. (2016) Discovery of a new type of scaffold for the creation of novel tyrosinase inhibitors. *Bioorg Med Chem.* 24(18):4509–4515.
- Şöhretoğlu D, Sari S, Barut B, Özel A. (2018) Tyrosinase inhibition by some flavonoids: Inhibitory activity, mechanism by in vitro and in silico studies. *Bioorg Chem.* 81:168–174.
- Sugimoto Kazuhisa, Nishimura T, Nomura K, Sugimoto Kenji, Kuriki T. (2003) Syntheses of arbutin-alpha-glycosides and a comparison of their inhibitory effects with those of alpha-arbutin and arbutin on human tyrosinase. *Chem Pharm Bull (Tokyo).* 51(7):798–801.
- Yin S-J, Si Y-X, Chen Y-F, Qian G-Y, Lü Z-R, Oh S, Lee J, Lee S, Yang J-M, Lee D-Y, Park Y-D. (2011) Mixed-type inhibition of tyrosinase from *Agaricus bisporus* by terephthalic acid: computational simulations and kinetics. *Protein J.* 30(4):273–280.
- Zolghadri S, Bahrami A, Hassan Khan MT, Munoz-Munoz J, Garcia-Molina F, Garcia-Canovas F, Saboury AA. (2019) A comprehensive review on tyrosinase inhibitors. *J Enzyme Inhib Med Chem.* 34(1):279–309.